SCALE EFFECTS IN ANIMAL LOCOMOTION

Based on the Proceedings of
an International Symposium held at
Cambridge University, September 1975

Edited by

T. J. PEDLEY

Department of Applied Mathematics and Theoretical Physics,
University of Cambridge, England

1977

ACADEMIC PRESS

LONDON NEW YORK SAN FRANCISCO

A Subsidiary of Harcourt Brace Jovanovich, Publishers

27. Model Tests on a Wing Section of an Aeschna Dragonfly.

B. G. NEWMAN
Department of Mechanical Engineering, McGill University, Montreal, Canada.

S. B. SAVAGE AND D. SCHOUELLA
Faculty of Engineering, McGill University, Montreal, Canada

ABSTRACT

The chord Reynolds number of a dragonfly wing flying at high speed is of the order of 10^4. It is well known that aerofoils at moderate incidence experience an increase of drag coefficient and a decrease of lift coefficient as the Reynolds number is reduced below a critical value of about 5×10^4 and that this is associated with complete separation of the laminar boundary layer.

The aerofoil section of the dragonfly is unusual, as indicated by Fig. 1a which is a sketch of a photograph of the section just inboard of the nodus on the wing of *Aeschna Eremita.*

Attention is drawn to the minute saw-teeth on each web of the *T* section which forms the leading edge (costa), and the spurs on both sides of the matrix which supports the rear membrane. The saw-teeth very likely act as turbulators to promote transition in the separated shear layer and subsequent reattachment of the boundary layer in a turbulent state. Smoke tunnel studies of the wing section support this hypothesis. Trapped vortices are observed in the *V* sections at low incidence, and at high incidence (about 10°) the flow is observed to reattach to the rear cambered membrane; the leading-edge separation bubble is then greater than half a chord in length. The purpose of the spurs which are roughly the height of the viscous sub-layer for the reattached flow, is less obvious.

The average flapping frequency in forward flight (about 10 m s^{-1}) is roughly 25 Hz (Nachtigall[12]) so that in one cycle the wing moves forward about 40 chord lengths. It is therefore postulated that the aerodynamics may be usefully studied, at least initially, on a static wing in steady flow.

Indoor free-flight tests have been made on two sizes of model glider with a similar wing section. Under stroboscopic illumination flights have been photographed using a long time exposure. With reflectors placed on the model and above the horizontal floor the flight altitude, flight-path angle and speed have been measured in steady

flights for various trim conditions. From this data the lift coefficients and drag coefficients as a function of angle of attack and Reynolds number may be estimated. The results show the dragonfly wing section to be very efficient and comparable to a very-high-performance, low-Reynolds-number aerofoil, fitted with an artificial turbulator.

INTRODUCTION

In his book "Structure-Form-Movement" Hertel[7] describes the membranous wings of a large dragonfly (*Aeschna Cyanea*). He comments on the pleated structure near the leading edge which is composed of strong veins at top and bottom joined by thin membranes (Fig. 1(a)). He notes that the chord Reynolds number of *Aeschna* flight ($\mathrm{Re} = U_\infty c/\nu$, where U_∞ is the flight speed, c the chord length and ν is the kinematic viscosity of air), which is typically $0{\cdot}5$–$1{\cdot}5 \times 10^4$, conventional aerofoils become less efficient than curved plates because the laminar boundary layer separates completely. It is then very advantageous to promote transition from laminar to turbulent flow in the boundary layer by means of trip wires or other devices. The dragonfly wing probably does this by forcing separation near the leading edge. Transition occurs much sooner in a separated shear layer, which then reattaches well before the trailing edge as a turbulent boundary layer: in this form it is capable of advacing against a higher pressure rise (higher by a factor of about 10) before separating again. Thus maximum lift is increased and form drag is reduced. Hertel also comments on other features of the wing: the T shaped leading edge (costa) with three rows of serrations which may act as turbulators to promote transition still further in the separated shear layer; the hairlets at the base of each serration; the small spurs which are scattered on the polygonal matrix of veins that form the rear 2/3 of the wing; and also on the chordwise veins near the leading edge.

The present investigation was undertaken to obtain quantitative information on the aerodynamics of the dragonfly wing and to determine whether some of these particular wing features have any aerodynamic significance. The broad aim is to improve the design of aerofoils at Reynolds numbers of about 10^4, where there are applications to model aircraft, and to low Reynolds number turbines and compressors (Charwat[3]). A wing section

FIG. 1(a). Sketch of dragonfly wing section.

FIG. 1(b). Chosen dragonfly wing section.

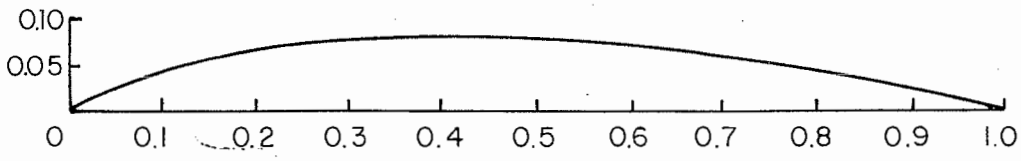

FIG. 1(c). McBride B-7 aerofoil section.

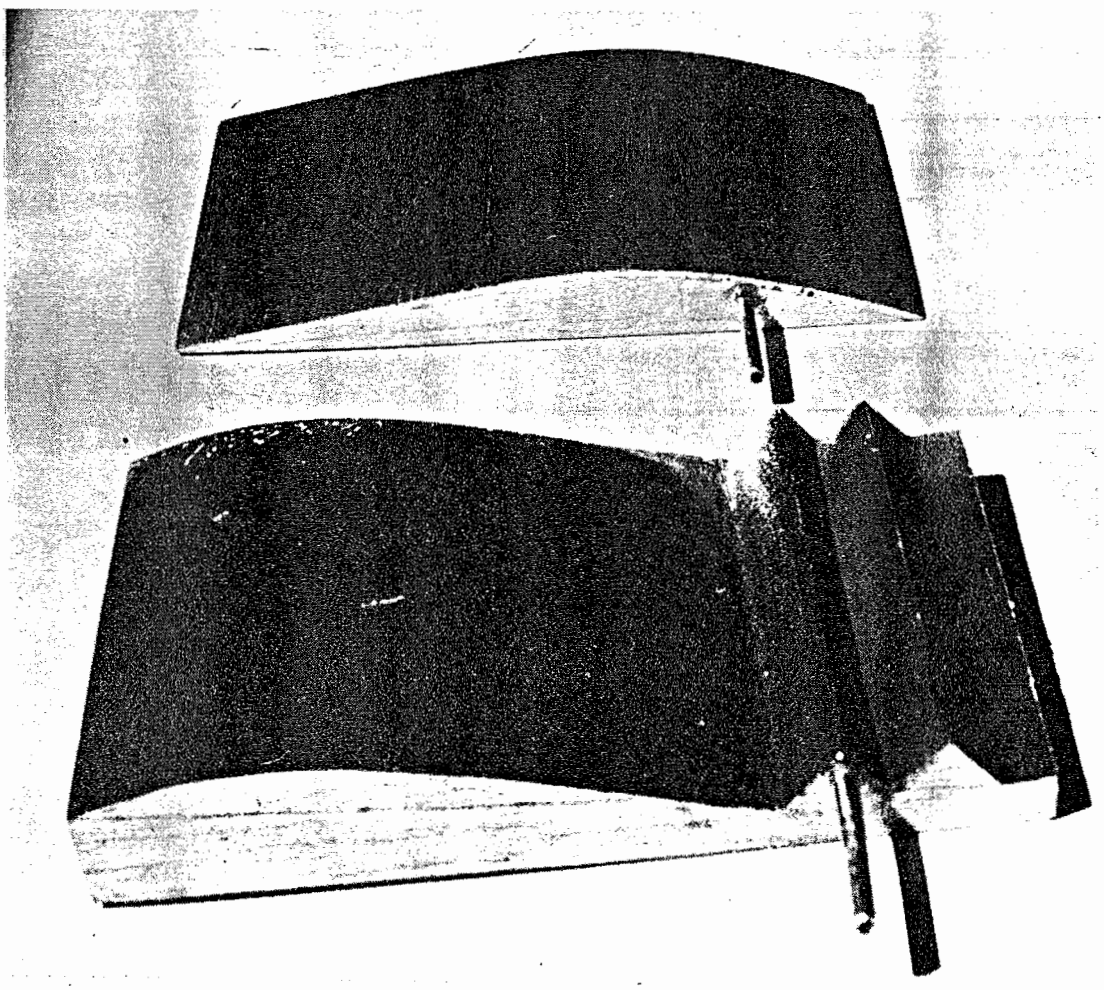

FIG. 2. McBridge B-7 and dragonfly smoke-tunnel models.

just inboard of the nodus (see Fig. 1b and Needham and Westfall[13] for a description of the various parts of the wing) of the fore wing of *Aeschna Interrupta* was chosen, since it was similar to the section of *Aeschna Cyanea* shown by Hertel. The wing was sectioned and scaled off by Paul Hayward from photographs which he took of a fairly old specimen (about 10 years old). A fresher specimen was not available at that time, but wings preserve well. This section was then used for flow visualisation on a similar tunnel model (Fig. 2) and for the wings of a model glider of aspect ratio 8 (Fig. 3).

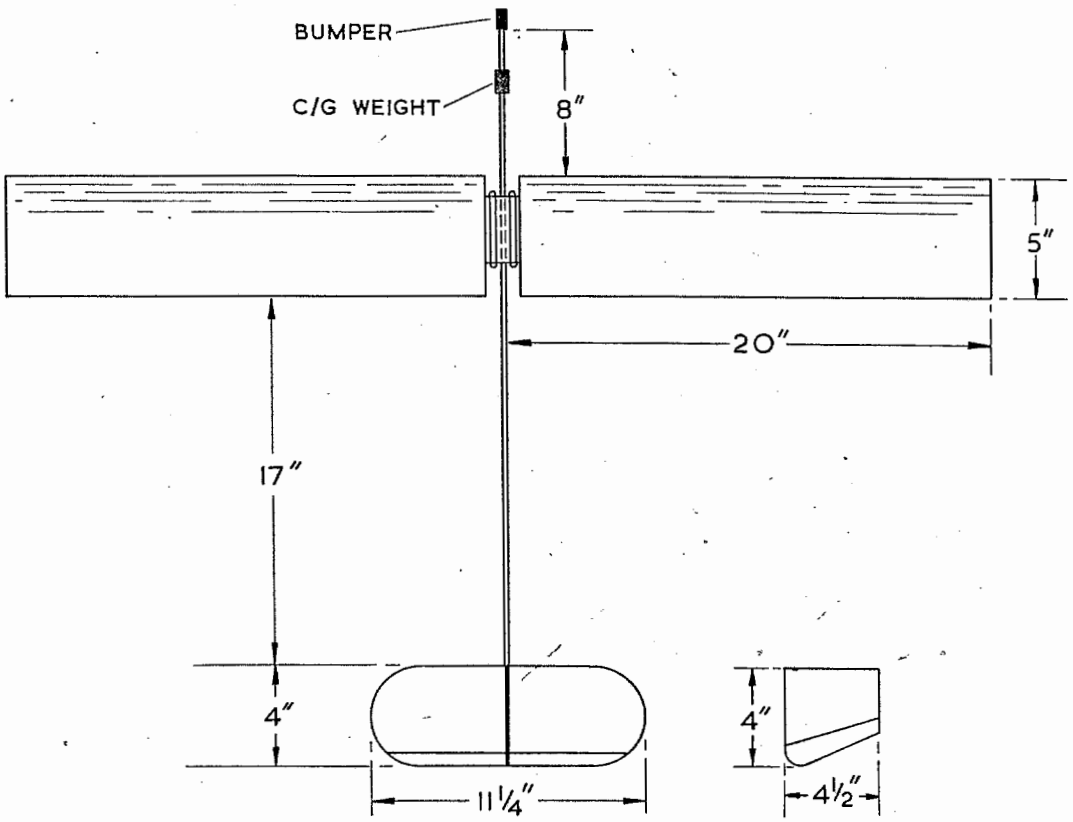

FIG. 3. Planform of large model glider (small model half-size but tail surfaces have rectangular planform). 1″ = 2·54 cm.

This glider was flown indoors using stroboscopic illumination and photography with long exposure to give flight speed, altitude and angle of attack. In addition, pictures of the detailed wing features of an Aeschnida and Libellulida dragonfly have been taken with a scanning electron miscroscope. Comparative pictures of a damselfly (a *Coenagrion*) have also been taken.

From an entomological viewpoint the above approach may seem naive, for Odonata are wonderfully complex. They have strong muscles which directly and independently flap the fore and hind wings, and weaker muscles which

control the relative positions of the main structural spars (costa, subcosta, radius, media and cubitus) (Pringle[17]). Thus the angle of attack, twist and camber are controlled to some extent from the root. Unlike birds there are no muscles within the wing itself. However, the main ribs must be fed with blood to supply nutrient to the various sensors which detect structural stretch, or the movement or rate of movement of hairs and diaphragms. Moreover, the blood supply can probably be greatly increased in order to straighten the ribs after they have been accidentally bent, in much the same manner as the wing was originally deployed when the full-grown nymph (instar) blossomed into the dragonfly.* Wing shape, therefore, depends on muscle control and internal fluid pressure in the rib, as well as the aerodynamic load on the wing. In addition the inertia loads due to flapping change the wing geometry (Weis-Fogh and Jensen[22]). In this connection the build-up of chitin on the leading edge near the wing tip (pterostigma) is no doubt significant as a mass which changes the inertia loading (Norberg[15]). The carboniferous relatives of the dragonfly which had a span of almost 0·75 m were apparently gliders, and both the nodus and the stigma were absent (Corbet, Longfield and Moore[5]).

The wing shape of the living insect may therefore be different from that of a dead specimen. The remarkable photograph of an *Aeschna* landing, which is presented by Nachtigall,[12] indicates that the camber in flight may be somewhat less than that of the sectioned wing of the dead insect. Thus the geometry we chose may be too highly cambered, and moreover it is specific to a particular spanwise position.

The flapping frequency is about 25 Hz at typical fast forward speeds of $10\,m\,s^{-1}$ (a maximum of $15\,m\,s^{-1}$ is quoted in the literature). Thus with a chord of 0·1 m, the wing travels forward 40 chords in one complete flap of the fore wing. It is perhaps not unrealistic therefore to investigate the efficiency of a typical aerofoil section in *steady* flow. The same assumption was justified in detail for the locust by Weis-Fogh and Jensen.[22]

The low flapping rate of the wings of both dragonflies and damselflies makes them particularly suitable for a quasi-steady study of wing efficiency. The smaller insects generally have a much higher flapping rate (several hundred Hz, increasing to about 1000 Hz for midges: British Museum[1]), and this is presumably one way of increasing the Reynolds number. The finite time required to build up a wing stall is also probably used to advantage. The low-speed flappers such as butterflies and moths (Lepidoptera) hook their wings together to avoid mutual wing interference and to increase the wing chord; butterflies also appear to apply high wing loading (high lift

* One of us has bent the main ribs of both dragonflies and damselflies and found that they are restored within a second or so, and that the animal is capable of flight again in less than a minute.

coefficient) only for very short periods. Of all the slow flappers the dragonflies (Anisoptera) are probably the fastest and most manoeuvrable (Chadwick[2]); they prey on the smaller insects which, if it were not for the decrease of wing efficiency with reduced Reynolds number, would be more manoeuverable and would probably be able to avoid capture. Thus the dragonfly apparently uses very ancient solutions to the problem of reducing the critical Reynolds number at values of about 10^4.

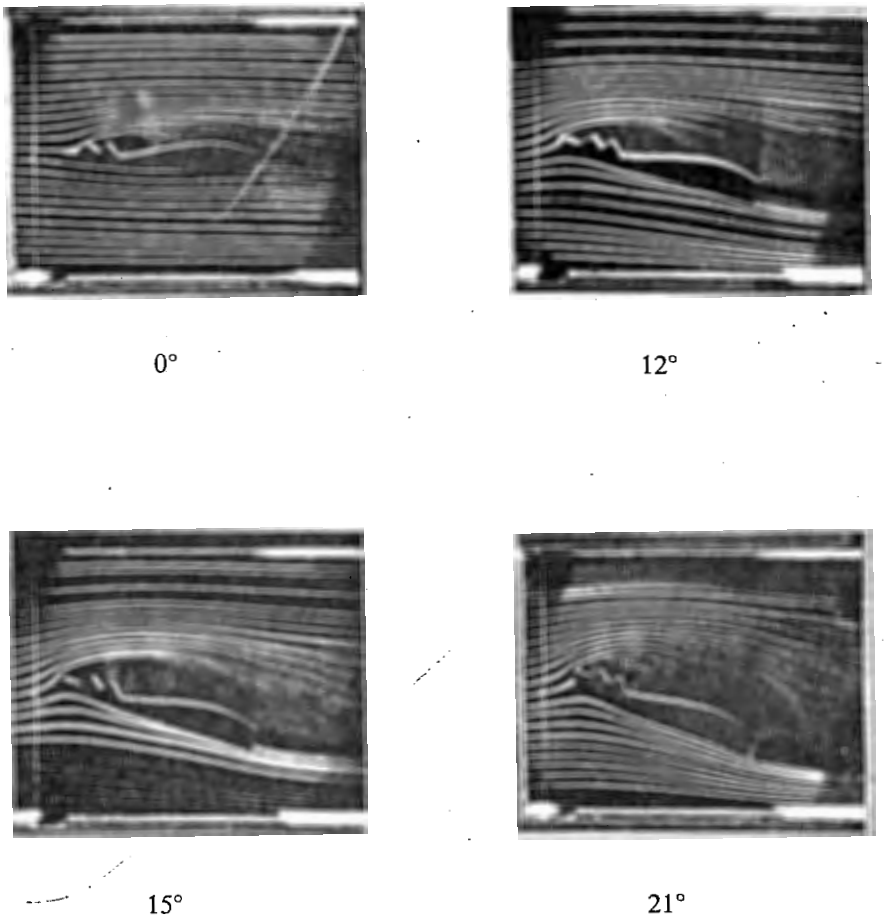

FIG. 4. Smoke tunnel pictures of the dragonfly aerofoil section at various angles of incidence

The present work relates to the theme of this conference in its investigation of optimum aerofoil shape at various Reynolds numbers around 10^4 and its subsidiary investigation of the maximum size of the spurs.

EXPERIMENTS AND RESULTS

Smoke Tunnel Observations

A two-dimensional model (12·7 cm chord, 8·9 cm span: Fig. 1) was built from thick balsa sheet and mounted in the McGill smoke tunnel (working section 8·9 cm × 17·8 cm): the flow was studied at various angles of attack at a Reynolds number of about 10^4. At 0° incidence of the chord line (see Fig. 4) a trapped vortex was observed in the first valley of the section. At 12° the flow was fully separated near the leading edge and reattached about 2/3 chord from the leading edge as a turbulent boundary layer. At 15° the flow was fully separated.

It was concluded that, *with the ends of the separation bubble sealed to maintain a low pressure within the bubble*, the wing section may indeed produce high lift at moderate incidence by promoting transition due to separation and reattachment of a large separation bubble.

Model Glider Tests

(i) *Experimental Procedures and Results*

As Reynolds number is decreased, most aerofoils at a fixed angle of attack experience a rather abrupt reduction of lift and increase in drag at a certain Reynolds number, which is usually somewhere between 3 and 8 × 10^4. This "critical" Reynolds number, which is analogous to the critical Reynolds number of about 3 × 10^5 for smooth spheres and cylinders in a low turbulence stream, depends upon aerofoil geometry, angle of attack, surface roughness near the leading edge and wind-tunnel turbulence level. Roughly speaking, raising the free stream turbulence level decreases the critical Reynolds number; the reasons are well understood. The higher turbulence level moves transition forwards, which delays separation. Since we thought that the unusual section of the Dragonfly wing with its pleats (which are found also on other insects, such as the locust), serrated leading edge (other types are also found) and spurs (not fully investigated) had evolved to have a low critical Reynolds number it was necessary to eliminate the effect of wind-tunnel turbulence. Accordingly free-flight tests were made indoors in the still air of the Sir Arthur Currie Gymnasium at McGill, thus effectively reducing the ambient turbulence to zero. Although the tests and data reduction are more tedious than wind-tunnel tests, one can obtain lift and drag coefficients as functions of angle of attack.

Two model gliders were constructed (Fig. 3), one having a span of 1 m, and designed to fly at a typical Reynolds number of 4 × 10^4, and the other half this size, more or less scaled as to weight and designed to fly at a Reynolds

number of 1×10^4. The latter is the value typical of high-speed *Aeschna*. The first model also had interchangeable wings so that the "dragonfly" wing performance could be compared with that of a more standard curved-plate aerofoil, the McBride B-7, an old section aeromodellers nonetheless consider to have a high performance near its critical Reynolds number. A comparison of the two sections is shown in Figs 1 and 2.

The wing with the dragonfly aerofoil was tested both with and without a correctly-scaled leading-edge turbulator which was machined on a screw-cutting lathe to resemble the serrated costa of the dragonfly closely. Wing end plates could also be added, since it was felt that they would help to "cap" the leading-edge separation bubble in the smoke-tunnel photographs at large angle of incidence. Note too that, whereas the model wings had a constant chord and section, the dragonfly wing pleats are swept back towards the tips and there are spanwise variations of section and chord.

Only the dragonfly section was tested on the smaller model, the purpose being to investigate the effect of reduced Reynolds number on performance.

The models were trimmed to fly at constant speed in various straight glide paths, and thus at various angles of attack of the wing, by adjusting the horizontal tail surface and a moveable nose weight (on the larger models) to change the position of the centre of gravity while keeping the total weight constant. The models were launched from a height of about 5·5 m above the gymnasium floor. Although a special launch mechanism was built for the gliders it was found to be quicker, simpler and more accurate to have them hand-launched by one of us who is an experienced aeromodeller. The usual procedure was to trim the model close to the stall condition and then successively trim it for steeper and steeper glide path angles. Test data were obtained by panning the gliding model with stroboscopic illumination in the darkened gymnasium while having two still cameras (a 35 mm Nikon for accurate data analyses and a Polaroid Land camera for "immediate" checks of flight quality) with the open shutter focussed on the glide path. With high speed black and white (3000 ASA) film and small reflectors on both the nose and tail of the fuselage (also on the rear wall to provide a horizontal reference), the flight altitude, flight path angle and flight speed could be determined. A typical photograph is shown in Fig. 5. The model is faintly visible in the photograph; the longer reflector is mounted on the nose and the shorter one near the tail. The horizontal reference reflectors are clearly visible in the bottom left and right of the photograph. Special calibration tests determined that the maximum photographic distortion of distances was 1·5% and the angular distortion was nil. Each photograph was rated A, B, C or D, or discarded depending on how closely the flight approached equilibrium conditions (i.e. constant speed U_∞, flight path angle β, and angle of attack α). Excellent quality was denoted by A, while B and C correspond respectively

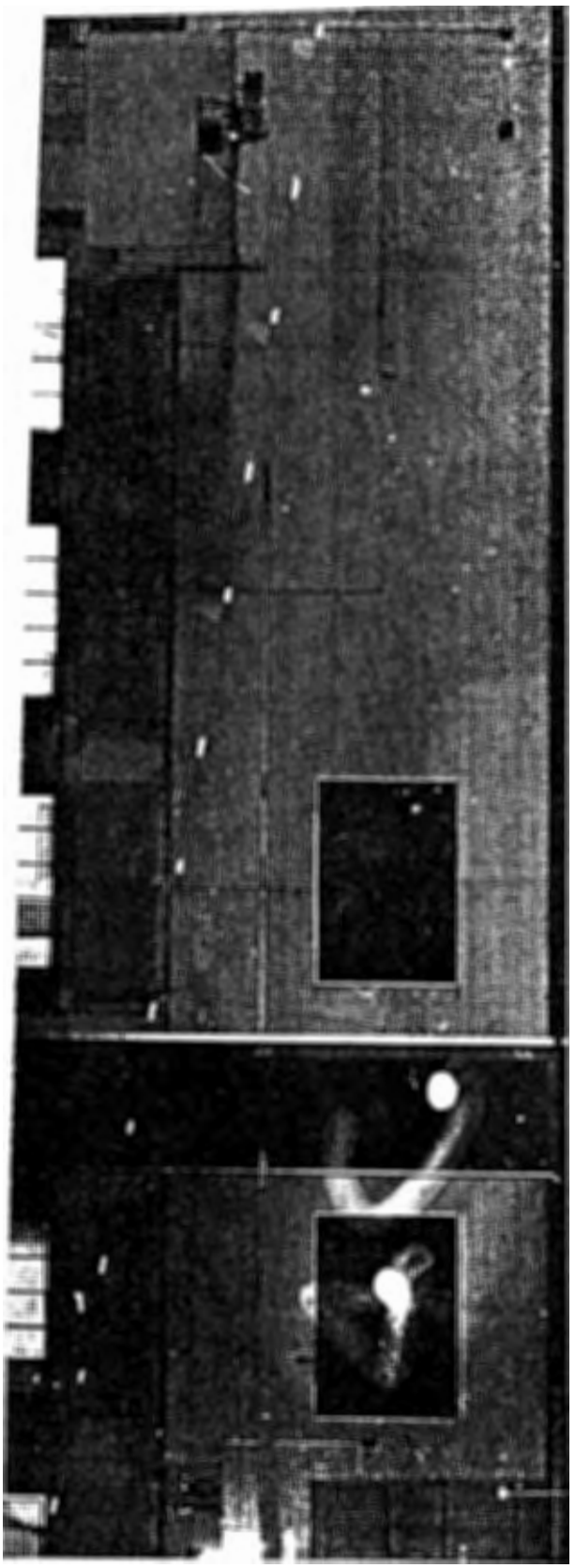

FIG. 5. Typical flight of the larger glider.

to most or half of the picture showing equilibrium flight and D corresponds to equilibrium being reached only at the edge of the field of view. The straightness of the flight also came into the assessment. In each case only the equilibrium position was used for data reduction purposes. This ranking, which is shown in some of the subsequent figures, is helpful in weighting various points when drawing curves through the data.

Each flight path yields particular values of α, β and U_∞ from which the lift and drag coefficients C_L, C_D for the complete glider can be obtained as follows

$$C_L = \frac{mg \cos \beta}{\frac{1}{2}\rho U_\infty^2 S}, \qquad C_D = C_L \tan \beta, \tag{1}$$

where mg is the weight of the model, S is wing surface area and ρ is the air density. These lift and drag coefficients include the effects of components other than the wing (i.e. the fuselage, horizontal and vertical tail etc.) and the effect of finite aspect ratio (i.e. the induced drag). Thus they are peculiar to the particular models tested and cannot in this form be compared with "standard" aerofoil data of other wing sections. Therefore the data have been further reduced to obtain the lift and drag, minus induced drag, for the wing alone. The lift on the horizontal tail was estimated from the calculated downwash at the tail and an assumed variation of lift with angle of incidence for the tail. This tail lift was subtracted from the total lift to obtain the wing lift coefficient C_{LW}; the corrections were rather small as shown in Figs 7 and 10(b). The drag coefficients of the various glider components aside from the wing were estimated following procedures used for the prediction of aircraft performance; typical values are shown in Table I. The drag coefficients of the

TABLE I. Estimated drag coefficients for large model (span = 1 m) at $U_\infty = 4\,\mathrm{m\,s^{-1}}$

Item	C_D
Horizontal tail	
Skin friction	0·00380
Induced	0·00014
Rudder skin friction	0·0016
Tail and reflector interference	0·0006
Wing guy wires	0·0050
Fuselage skin friction	0·00026
Nose weight and bumper	0·0032
Nose reflector and wing support	0·0013
Total	0·0159
End plates	0·0026

components were subtracted from the glider drag coefficient $C_{D\,(\text{glider})}$ to yield the wing drag coefficient C_{DW}. The induced drag was calculated and subtracted to yield the drag coefficient of the wing alone, corrected to infinite aspect ratio, C_{D_0} (see Figs. 8(a), 8(b), 10(c) below).

(ii) *Discussion of Results*

Because of the manner of flight testing the data are not obtained at constant Reynolds number. It is simple to show that $\text{Re} \propto (mg \cos\beta/C_L)^{1/2}$. For the larger model (1 m span), where the trim was changed by adjusting the nose-weight keeping the total weight mg constant, the Reynolds number increased with decreasing C_L and increasing β (C_L increases faster than $\cos\beta$). The smaller model (0·5 m span) was so small that it was trimmed with small calibrated weights which were placed in a nose compartment. Thus the nose weight and with it the all-up weight was larger when the small model was trimmed at low C_L. Because of this the Reynolds number variation over a given range of C_L is rather more for the smaller model than for the larger models.

The results are displayed by means of three types of graph: plots of lift coefficient C_L versus angle of incidence α, plots of drag coefficient C_D versus α, and plots of C_L versus C_D (polar plots) derived from the first two. The former are straightforward to understand, and would show clearly, for example, the rise in drag and fall in lift which occur as α is increased above the stall angle (at any given Reynolds number). However, from the point of view of assessing a wing's aerodynamic performance, polar plots are extremely informative and are widely used by aerodynamicists; in particular, they allow one to see at a glance the maximum value of the lift–drag ratio, which, for constant efficiency of propulsion and constant rate of fuel consumption, determines the maximum range of a flying animal (see Lighthill's paper above), and the minimum gliding angle β (Eqn 1).

Large models (*dragonfly and curved-plate sections*). The Reynolds number for these tests ranged from about $3{\cdot}5 \times 10^4$ to 6×10^4. A complete model polar plot (of C_L versus C_D) for the plain dragonfly wing section is shown in Fig. 6. The C_L versus α curves for this model, for the dragonfly wing with turbulator, the dragonfly wing with both turbulator and endplates, and the McBride B-7 curved plate sections are shown in Fig. 7. The drag coefficients $C_{D\,(\text{glider})}$, $C_{D\,(\text{wing})}$ and C_{D_0} versus α for the plain dragonfly and the curved plate wings are shown in figs. 8(a) and (b).

Of particular interest are the "kinks" that occur in the C_L versus C_D, C_L versus α and C_D versus α curves for the plain dragonfly wing at a value of C_L of roughly 0·75 ,and $\alpha = 8°$. The drag coefficients also decrease with α

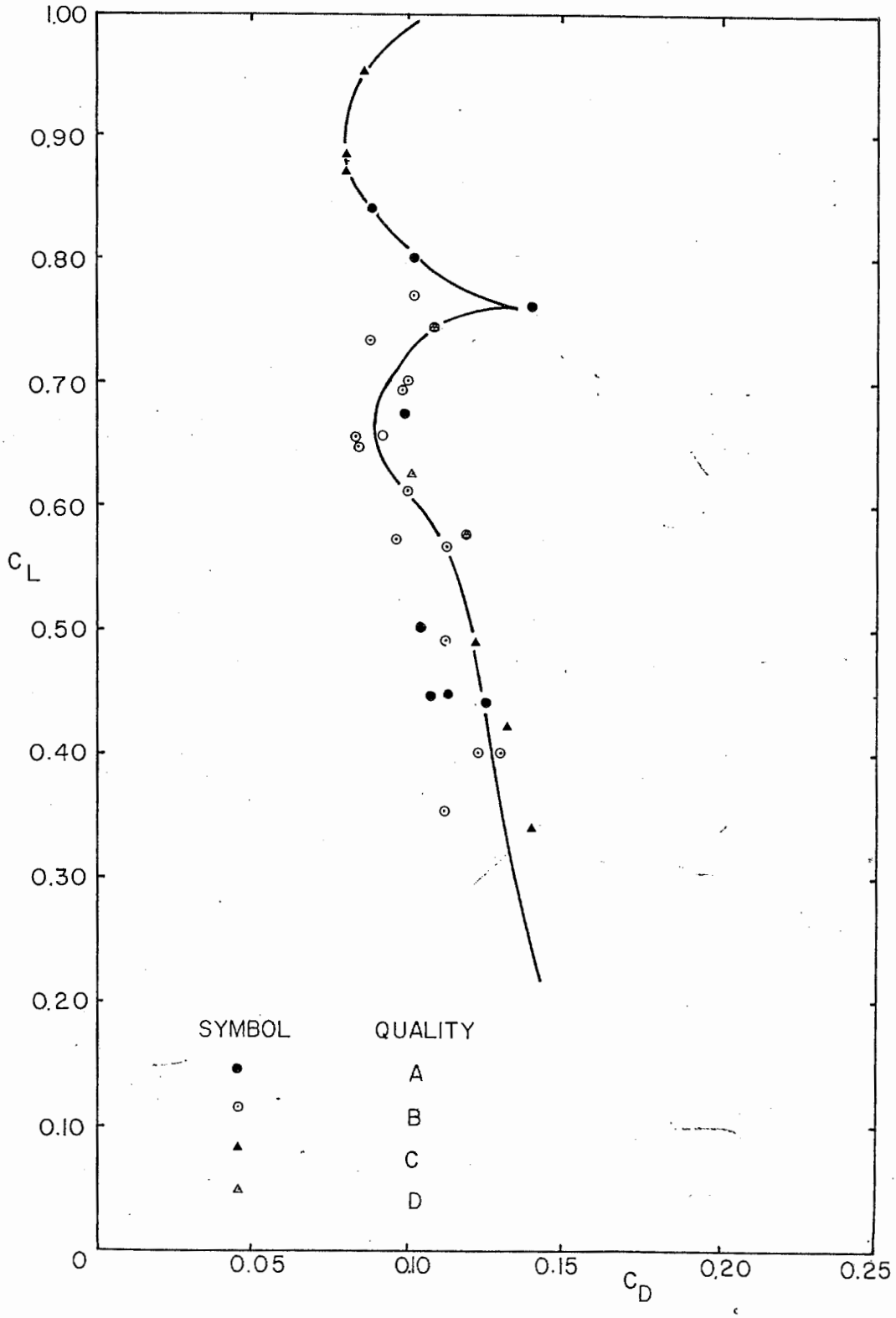

FIG. 6. C_L–C_D curve for plain dragonfly section—large model. Re $\approx 3{\cdot}5 \times 10^4$–$6 \times 10^4$.

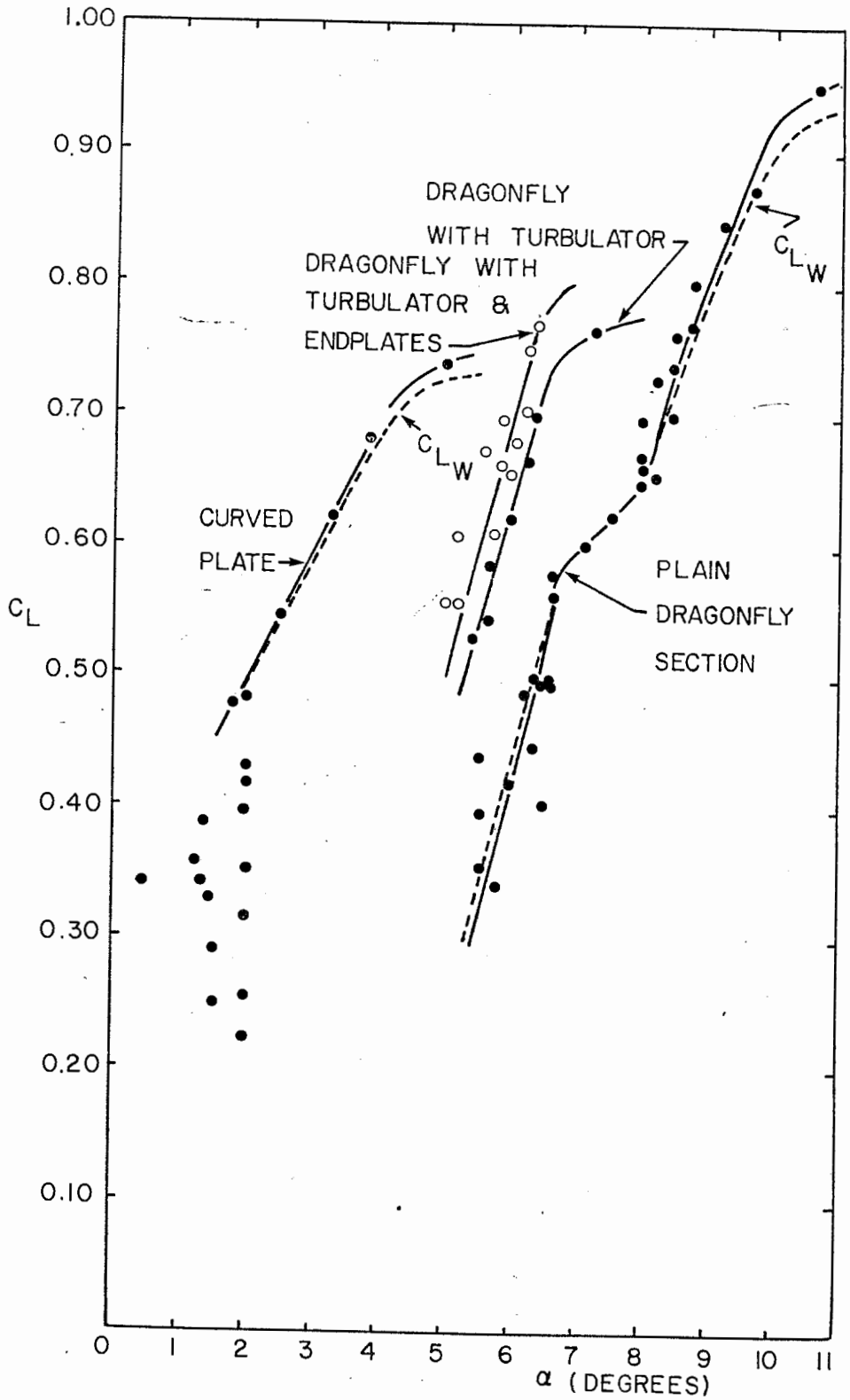

FIG. 7. C_L–α curves for large models with and without modifications and also the McBride B-7 aerofoil. Re ≈ 3·5 × 10^4–6 × 10^4.

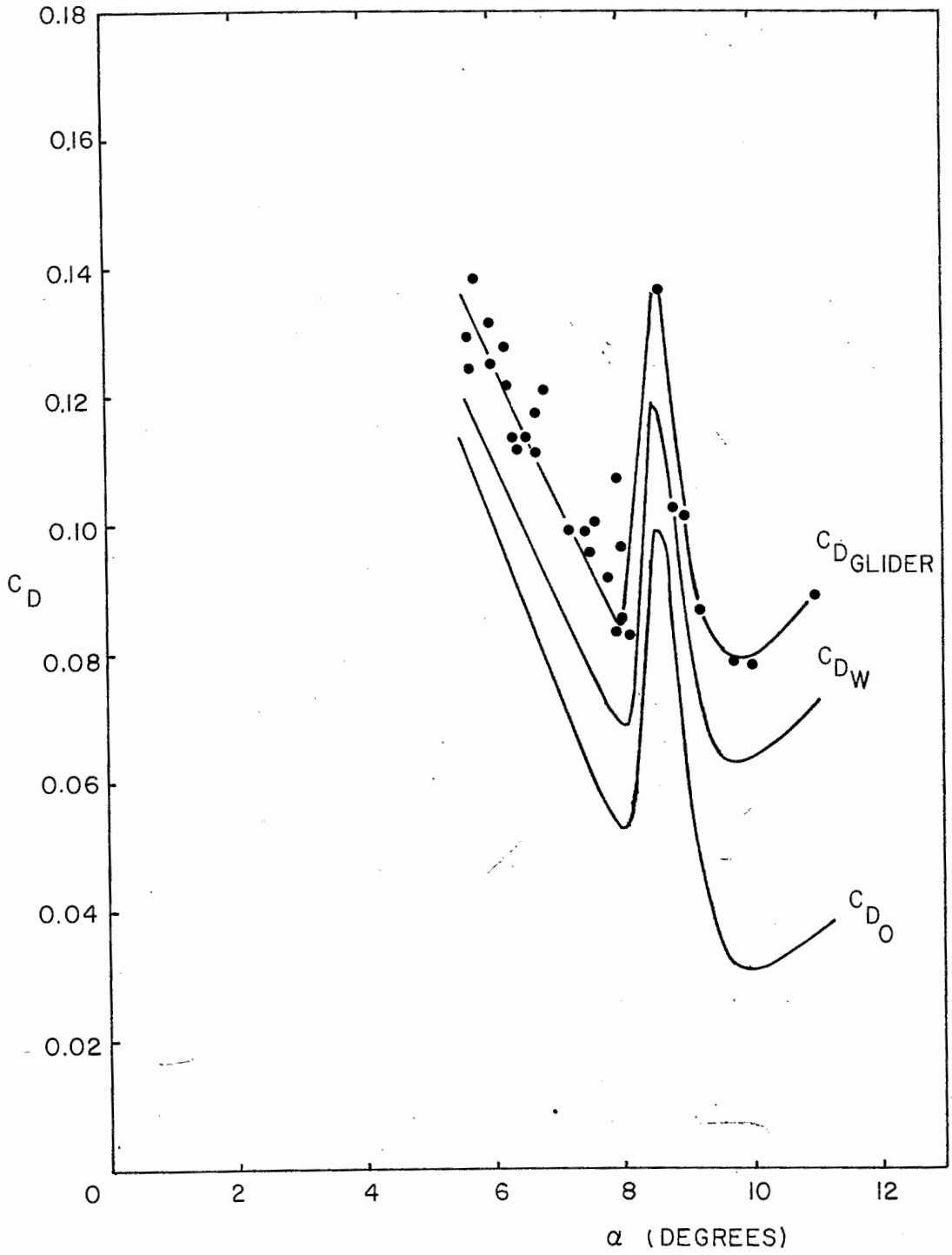

FIG. 8(a). C_D–α curves for large plain dragonfly section.

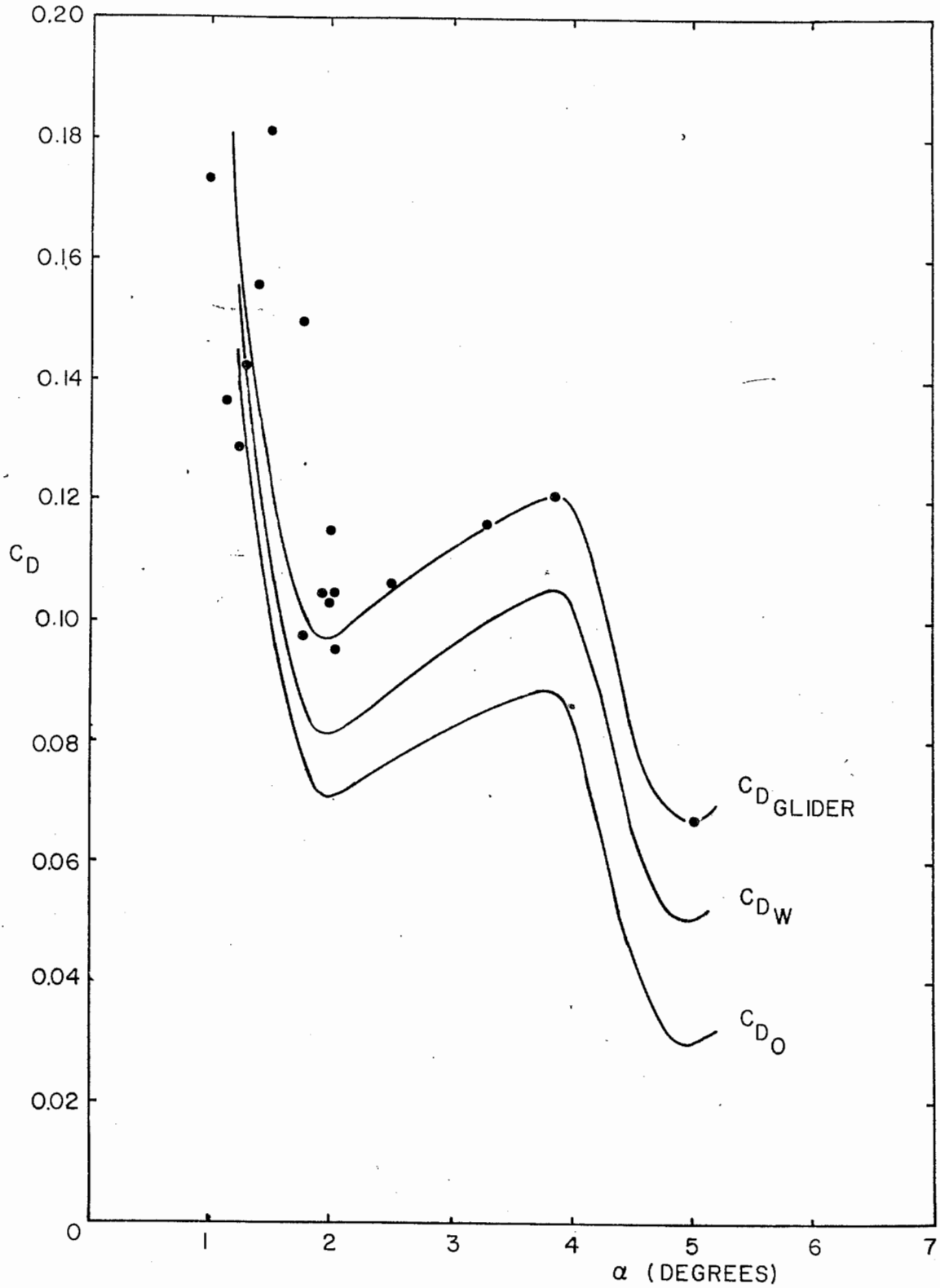

FIG. 8(b). C_D–α curves for the McBride B-7 aerofoil.

at smaller α. Both of these characteristics are sometimes noted for thin uncambered aerofoils at low Reynolds numbers (see for example Rabel[18]). There are relatively few aerofoil data for $Re < 10^5$ and many of these are unreliable because of wind-tunnel turbulence. Rabel has compiled most of this data.

It is seen that the kink in the C_L/C_D curve for the dragonfly model (Fig. 6) represents a significant variation in C_D at a more or less fixed value of C_L. In a steady glide the three forces, lift L, drag D and weight mg are in equilibrium. Moreover the lift is much greater than the drag and the glide angle β is small. The lift then approximately equals the weight and equations (1) become

$$C_L \simeq \frac{mg}{\frac{1}{2}\rho U_\infty^2 S}, \qquad C_D \simeq C_L \beta. \tag{2}$$

For any given configuration U_∞ is thus determined by C_L. Hence when C_D varies at a fixed C_L the model (and by inference the dragonfly) can fly at a constant speed and at various glide-path angles β. Such behaviour may be of great use to the dragonfly in pursuing and catching other insects in the longitudinal plane, a behaviour which is characteristic of the dragonfly when feeding.

The flow about the corrugated dragonfly wing section is a bit more involved than the flow about the plain wing, and a possible physical explanation of the aerofoil characteristics is as follows (see Fig. 9). At low α several separation bubbles are present, one (at least) in each pleat and a larger one on the rear undersurface. In region (1) the high lift-curve slope ($>2\pi$) may be associated with the change of effective camber as the bubble on the undersurface decreases in size with increasing α. C_D decreases as the wake narrows. In region (2) the bubbles are confined to the pleats, the lift-curve slope is reduced, probably due to boundary layer thickening over the aft portion of the wing. At (3) a large upper-surface bubble appears, increasing the lift and the drag, a feature which is aggravated by the decrease in flight Reynolds number with incidence. With further increase in α it is postulated that the critical Reynolds number is reached, transition in the separated shear layer occurs earlier, the bubble decreases in size and with it the drag. The flow finally separates completely at (4) and the wing stalls. These schematic diagrams should be compared with Figs. 7 and 8(a).

The effects of the turbulator are to increase the drag slightly and to increase the lift considerably at a given α before stall (Fig. 7). With the turbulator in place the "first" stall occurs at a higher C_L. It is likely that, as with the plain dragonfly wing, there is a "second" stall at higher C_L. The test procedure, in which the model was trimmed close to what appeared to be the stall and C_L successively decreased, may have caused us to miss the upper portion of

the polar. In this region (near the first stall) C_D changes rapidly with α and it was difficult to launch the model for a straight glide path. Even a slight misalignment could cause one half of the wing to have considerably higher drag than the other, inducing the model to veer off strongly to the left

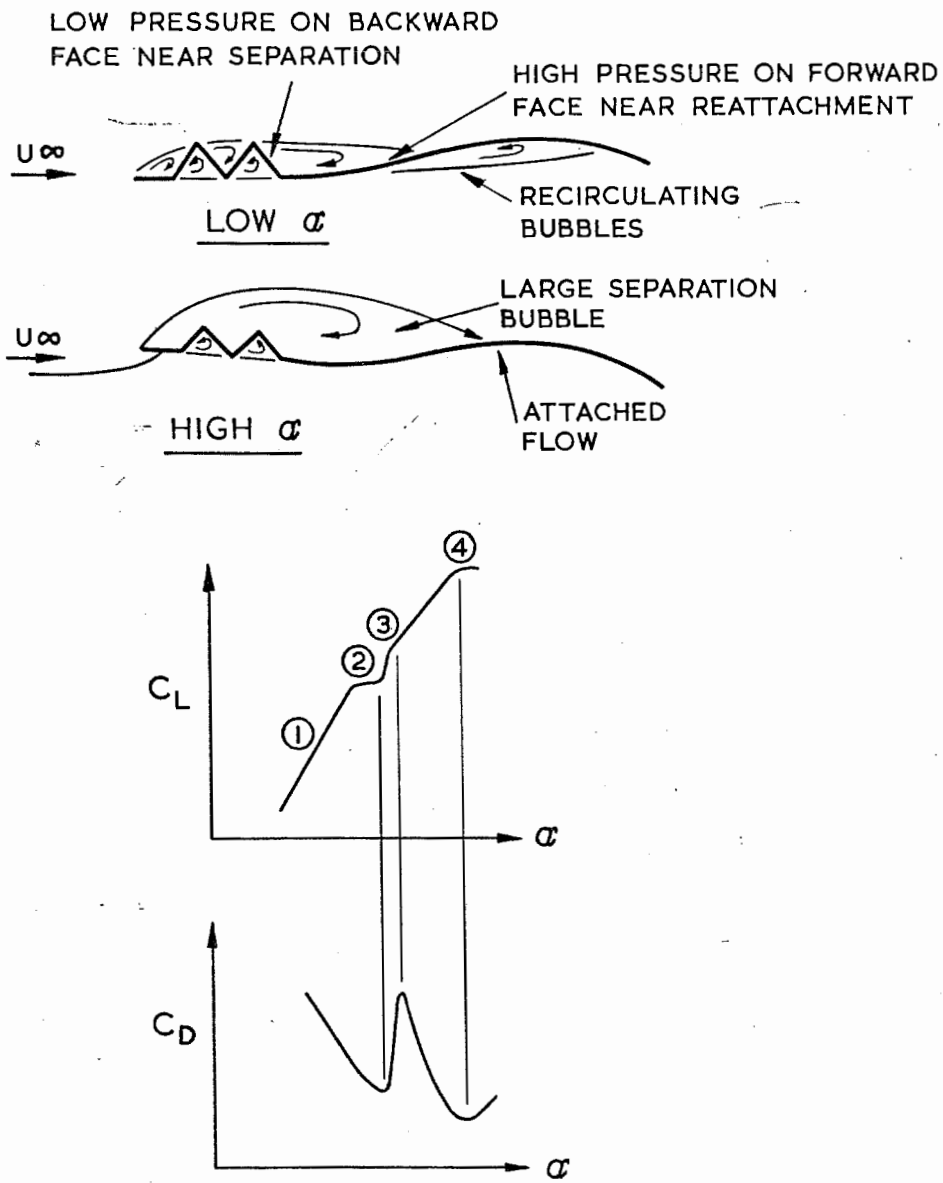

FIG. 9. Schematic diagram of flow and section characteristics.

or to the right. The cause of these difficulties was not realized during the flight tests and it was assumed that the model was turning because of loss of lift on one wing due to stalling.

Addition of the end plates to the dragonfly wing increased the drag because of the increase of area covered by the separation bubble. The lift at a given α was increased (Fig. 7), probably because the end plates closed or "capped" the leading-edge separation bubble and increased the camber effect.

The curved-plate wing has the same gross behaviour as the dragonfly section (Figs. 7 and 8(b)). The drag at low α is rather larger, probably because of a larger undersurface separation bubble. The stall may not have been reached; the curves at high C_L are uncertain because of the lack of data points. On the C_L versus α curves there is a great deal of scatter for $C_L < 0{\cdot}5$ (Fig. 7). It is likely that this is associated with hysteresis for the lower-surface separation bubbles whose size may depend on the flight-path history previous to the equilibrium portion of the flight. The concavity of the surface must play a significant part in this hysteresis for it does not seem to be present for the upper surface separation bubbles.

It is seen from Fig. 7 that the correction to C_L to account for the tail lift is quite small and from Fig. 8(b) that the wing produces the major portion of the total drag. It may also be noted that the lift curve slope, $dC_L/d\alpha$ of the dragonfly wing is very large (11 per radian) compared with the theoretical value of 2π per radian. This is also attributed to the separation bubbles. With increasing α the lower bubble size decreases and the upper bubble increases in size and both effects increase the effective camber. The effective aerofoil shape thus changes with α, giving rise to a lift-curve slope greater than the theoretical value.

Small model with dragonfly section. The smaller model, whose linear dimensions were half those of the larger model, flew at Reynolds number roughly a quarter as large as the larger model. The test data, which were obtained only for the plain dragonfly section, were reduced in the same manner as for the larger models (see Figs 10(a), (b) and (c)). There appear to be kinks in the curves for C_L versus C_D and C_D and C_L versus α at around $C_L = 0{\cdot}3$ ($\alpha = 4°$) and $C_L = 0{\cdot}65$ ($\alpha = 7{\cdot}5°$). From the curves it is not clear that the model was close to stalling in any of the glide tests and it is possible that higher lift coefficients could have been obtained before the wing stall. Curves of C_{LW} versus C_{D_0} for the plain dragonfly section on the large model (Re $\simeq 3{\cdot}5 \times 10^4$ to $2{\cdot}5 \times 10^4$) and the small model (Re $\simeq 1{\cdot}2 \times 10^4$ to $2{\cdot}5 \times 10^4$) are compared in Fig. 11. Surprisingly, the smaller model has a lower C_{D_0} for $C_{LW} < 0{\cdot}56$. To give some idea of the performance of the dragonfly section compared with other aerofoils, Fig. 12 shows C_L versus C_{D_0} for probably the highest-performance, low-Reynolds-number aerofoil chosen from amongst the reliable data compiled by Rabel.[18] This aerofoil is the Göttingen 803 with a wire turbulator placed 8% of the chord ahead of the leading edge. Data are

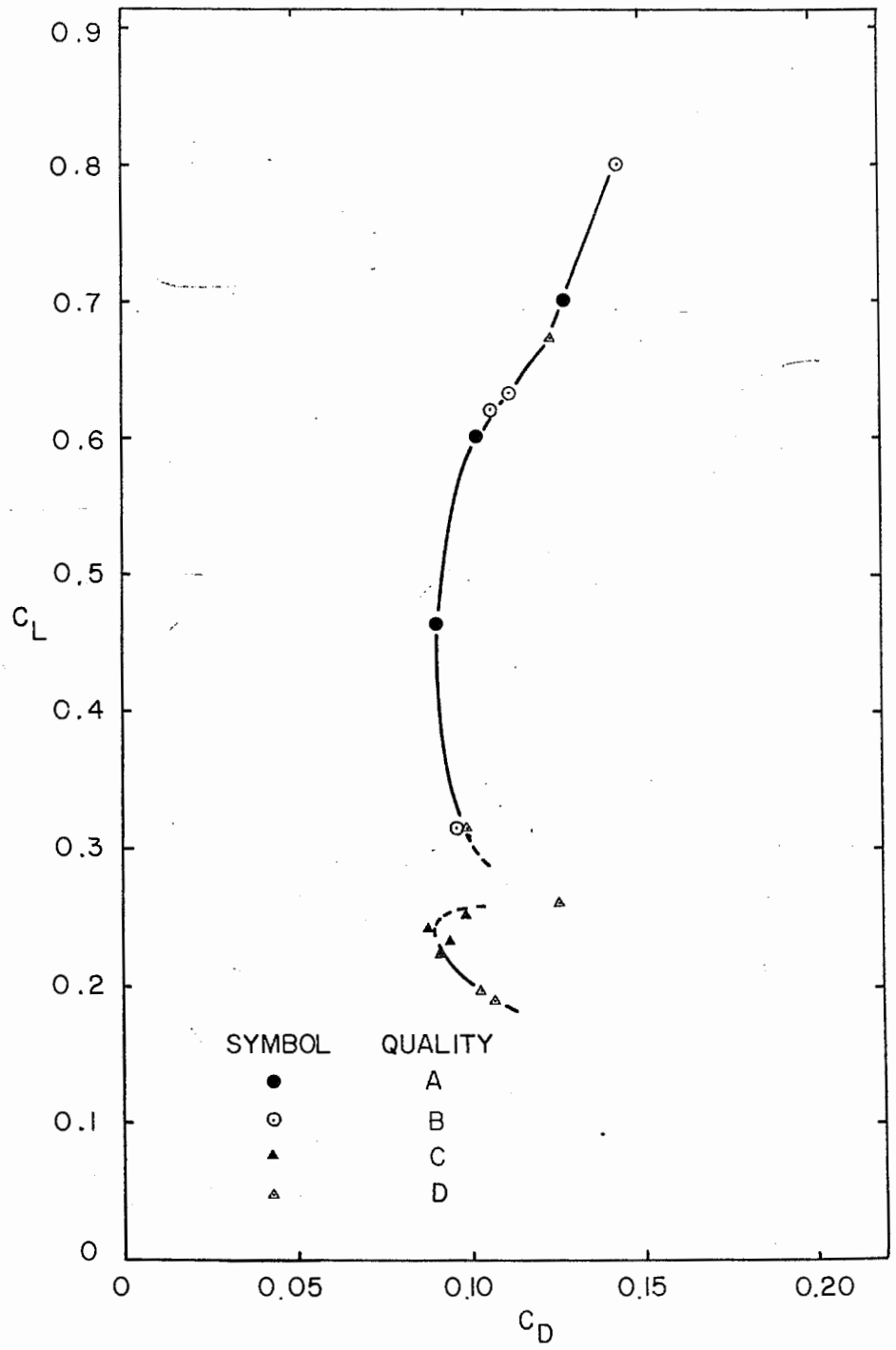

FIG. 10(a). C_L–C_D curve for plain dragonfly sections—small model.

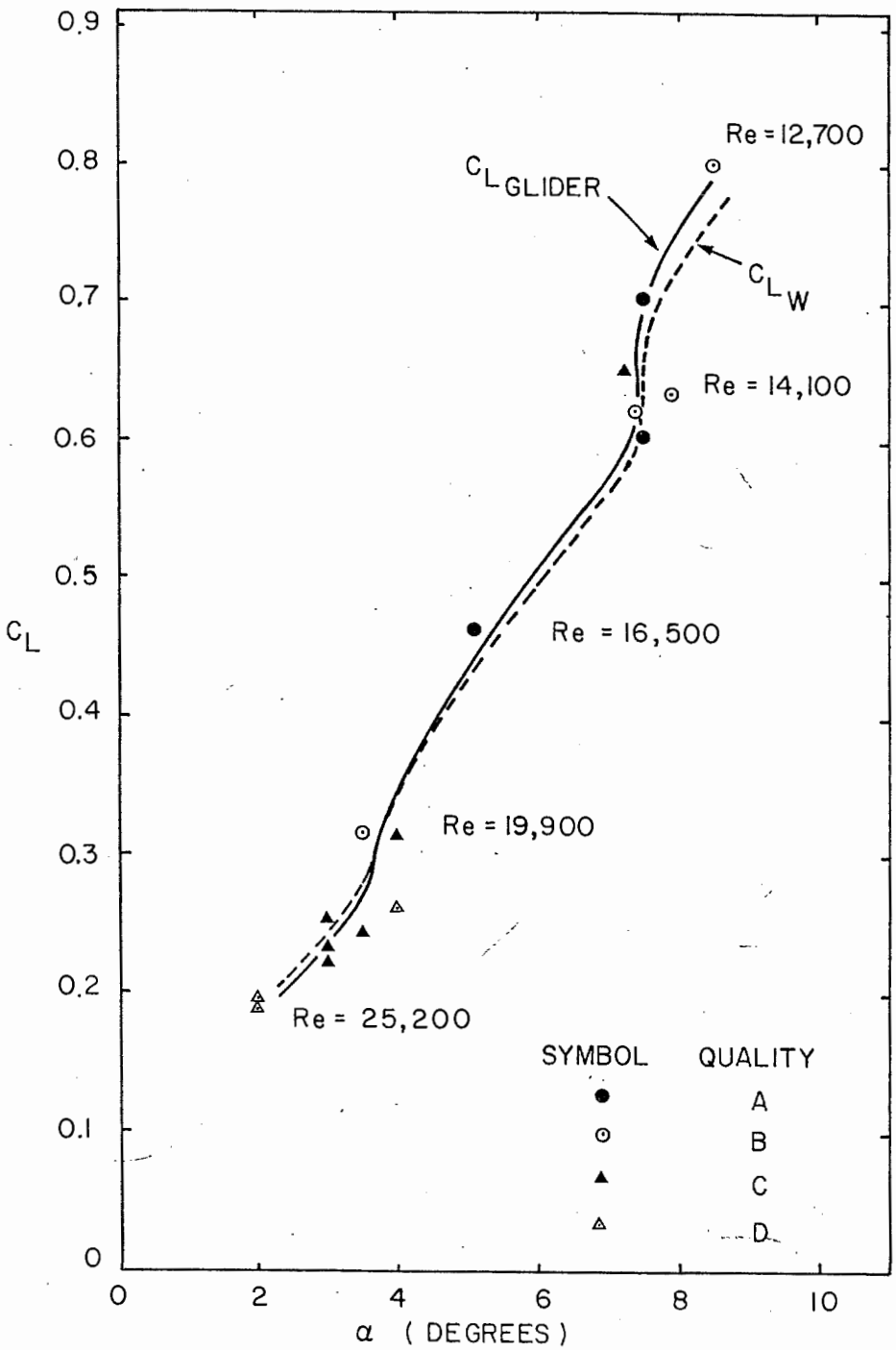

FIG. 10(b). C_L–α curves for plain dragonfly sections—small model.

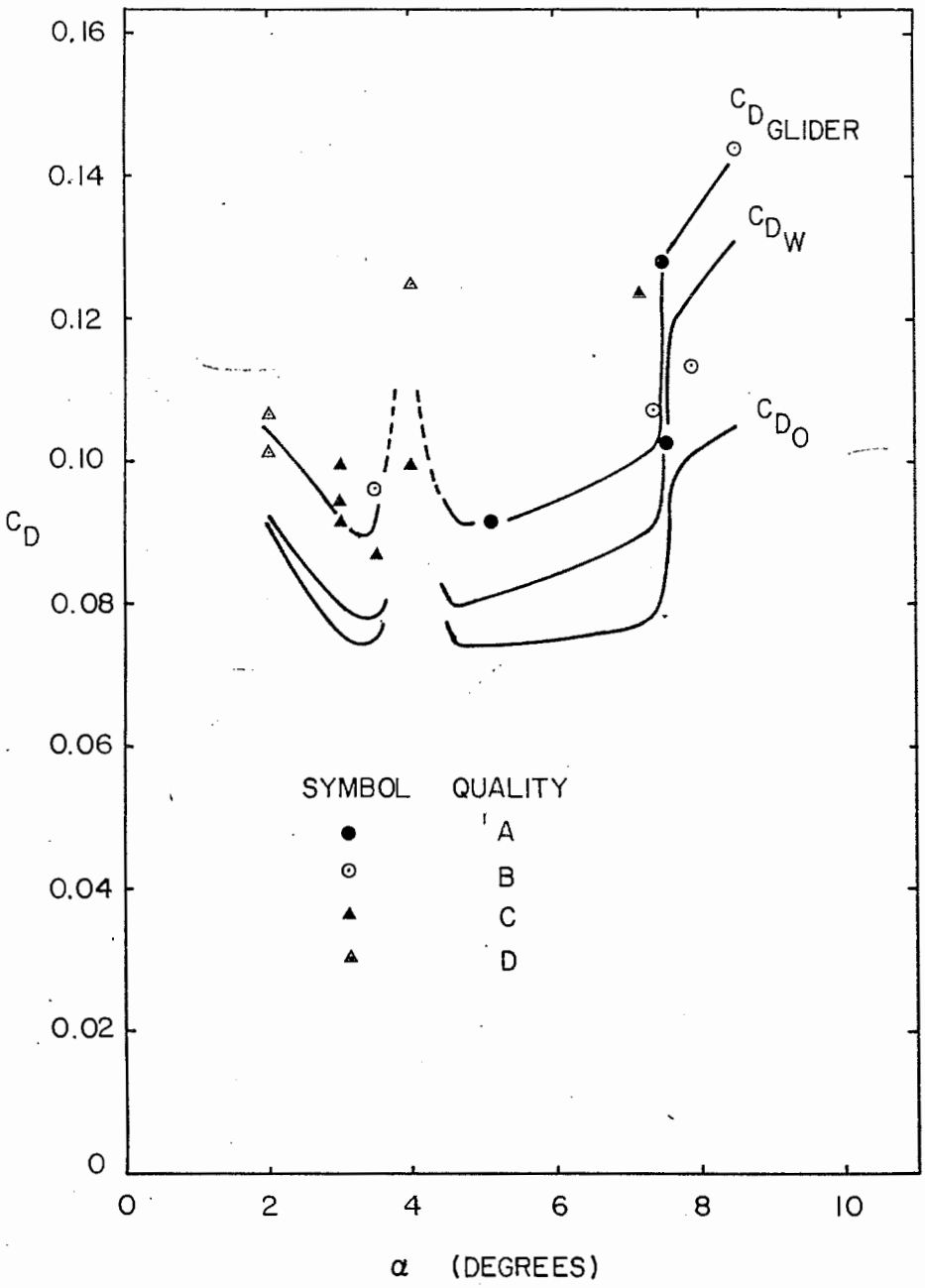

FIG. 10(c). C_D–α curves for plain dragonfly sections—small model.

shown for the aerofoil with and without the turbulator for several Reynolds numbers. The strong effect of Reynolds number and the beneficial effect of the turbulators are quite evident. After the abrupt performance drop at the critical Reynolds number, most aerofoils experience a more gradual, but still very marked, performance degradation with decreasing Reynolds number. Maximum lift to drag ratios (corrected to infinite aspect ratio) for standard,

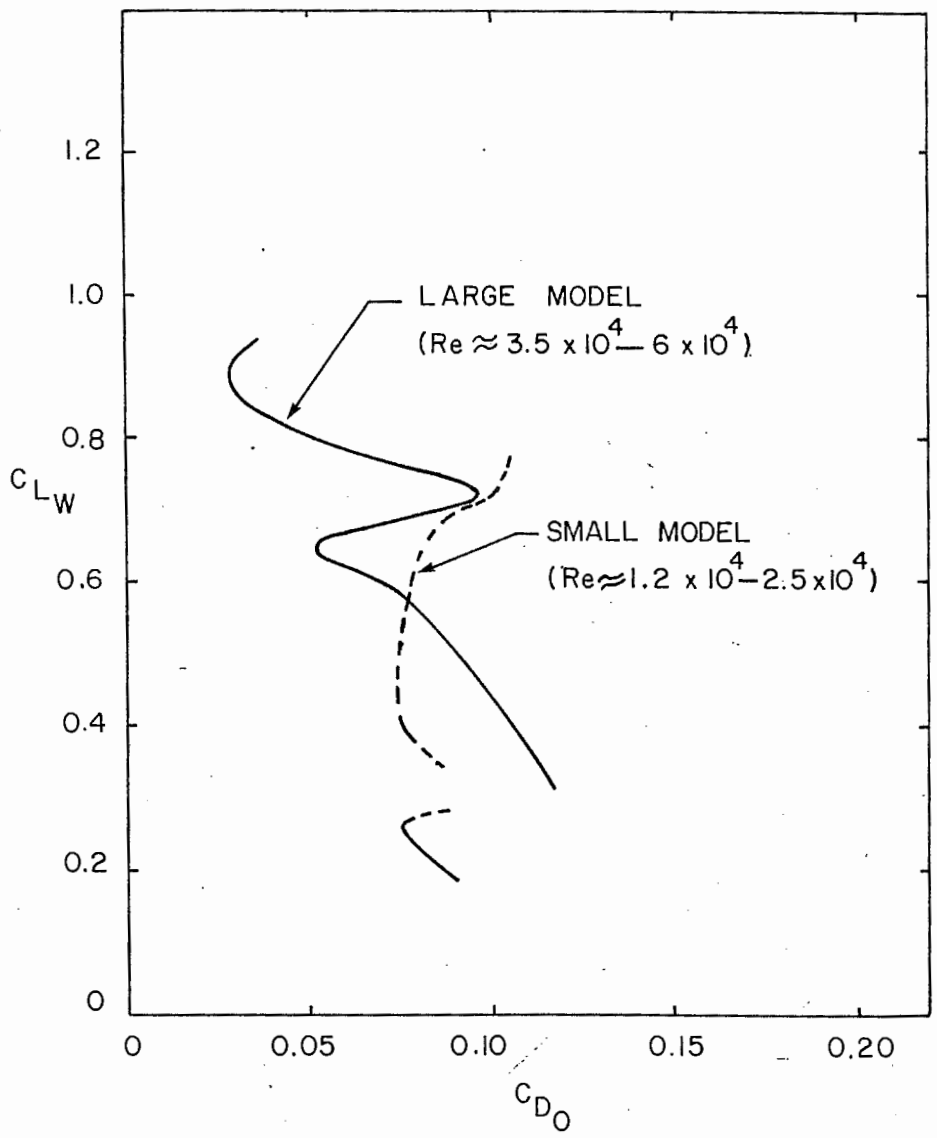

FIG. 11. C_L for the wing alone versus profile drag coefficient C_{D_0} of the wing alone, for both plain dragonfly models.

quite ordinary looking, aerofoils are typically as low as 5 (or even 2 for thick aerofoils) for Reynolds numbers around $2{\cdot}5 \times 10^4$. By comparison the Göttingen 803 with turbulator and the dragonfly section are very efficient aerofoils. In fact, the small dragonfly section (without turbulator) at the higher C_{LW} corresponding to $\mathrm{Re} = 1{\cdot}2 \times 10^4$ compares favourably with the Göttingen 803 with turbulator at a higher Reynolds number of $2{\cdot}5 \times 10^4$. It is very likely that the actual live dragonfly wing, containing features such as the serrated leading-edge, nodus with the change in aerofoil section, pleats swept back at wing tips, spurs or cones on wing surface etc., has a better performance than that shown in Fig. 10(a).

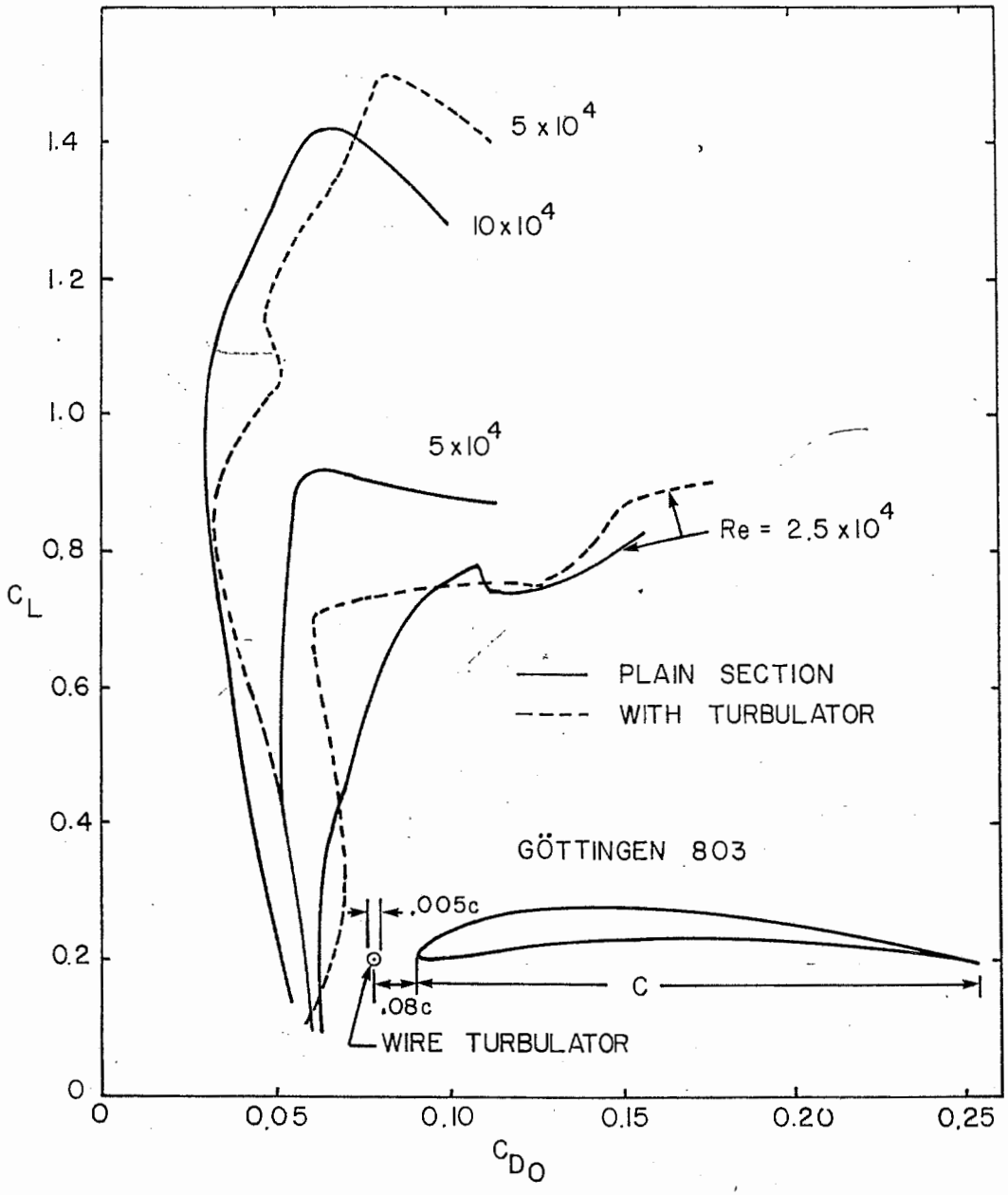

FIG. 12. C_L–C_{D_0} curve for Göttingen 803 aerofoil at low Reynolds numbers (Rabel[18]).

SCANNING ELECTRON MICROSCOPE PICTURES

Preliminary pictures were taken on a Cambridge Stereoxam 600 in the Soil Mechanics Laboratory at McGill University with the help of Dr. D. Sheeran. Uncoated specimens of a small *Libellula* were viewed at magnifications of up to 2000 and voltages of 7·5 kV. The specimens were damaged to some extent by the build-up of charge. However, the form of the spurs was

(*a*)

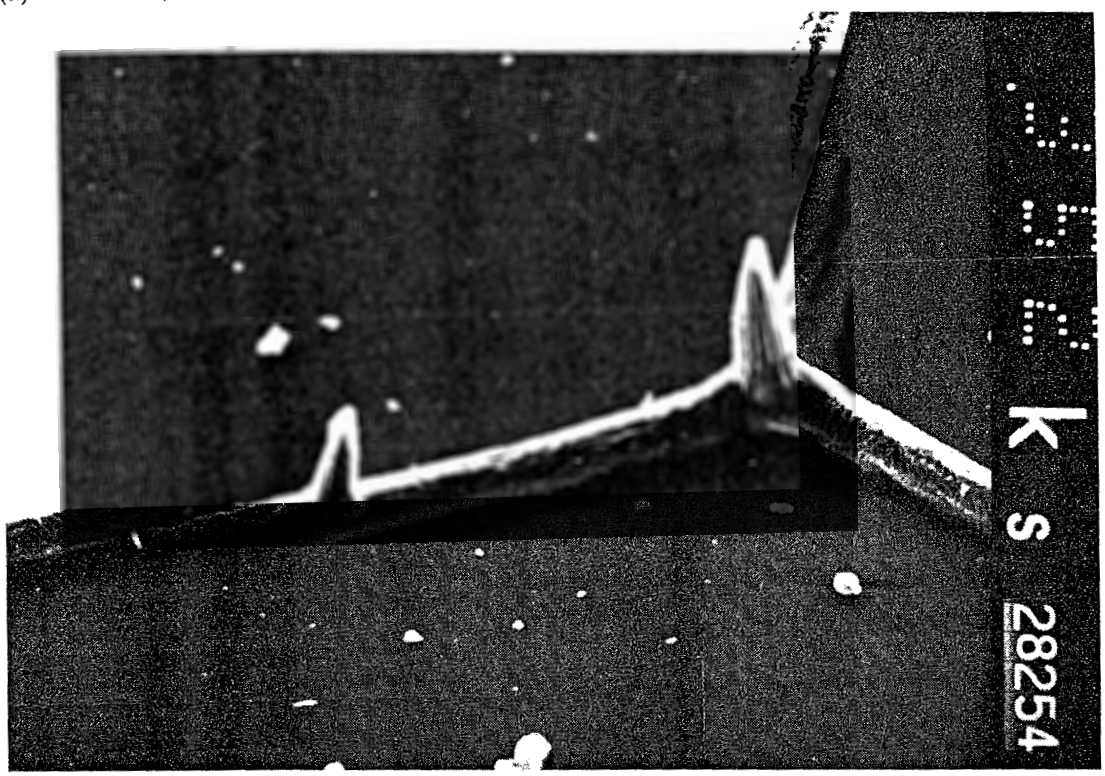

(*b*)

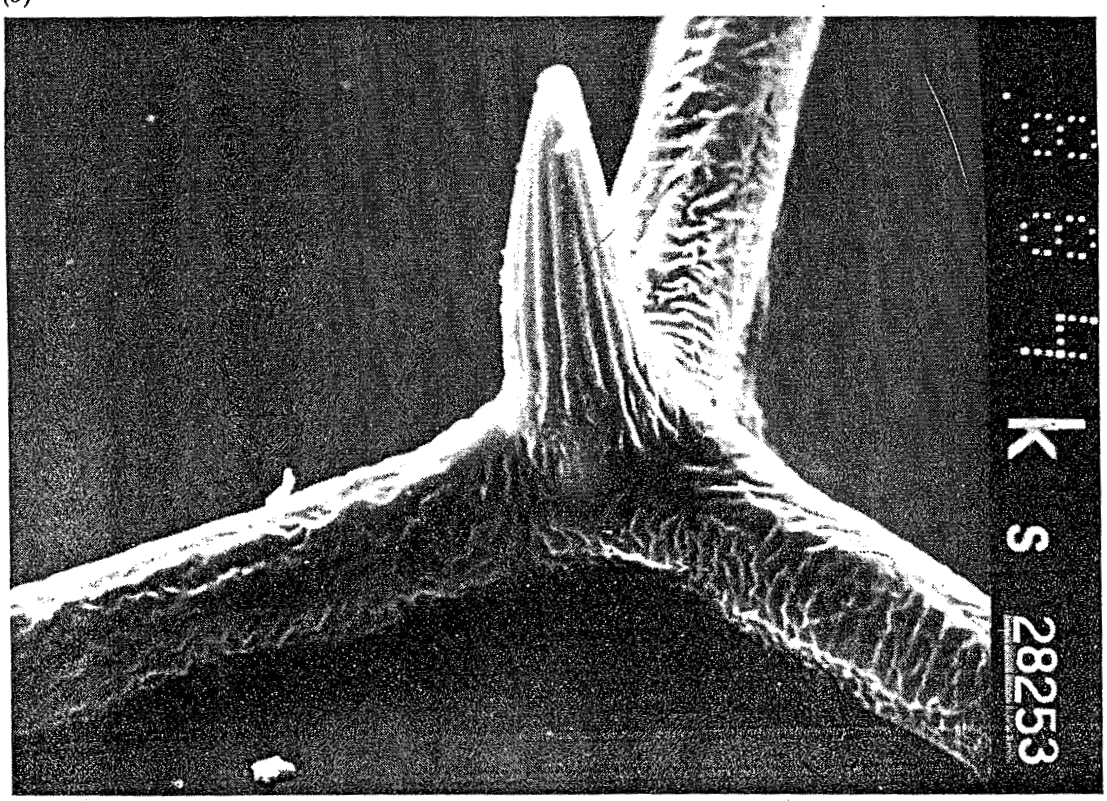

FIG. 13. Spurs on the upper surface of the fore wing of an *Aeschna*, at magnifications of (a) 352 and (b) 884.

clearly seen and they were essentially the same as the later ones shown here. The height of the spurs above the diaphragm was 55 μm.

Better quality pictures were taken on the larger instrument at the Pulp and Paper Research Institute of Canada by Gunther Seibel on specimens which were plated with gold–palladium. Two pictures of a spur at the joining of two veins about half way back along the upper side of the fore wing of *Aeschna Interrupta* are shown at magnifications of 352 × and 884 × in Figs 13(a) and (b). Similar pictures are shown of the underside of the hind wing of the same dragonfly in Figs 14(a) and (b) at magnifications of 144 × and 730 ×. The wing was viewed obliquely at 45°. The heights of the spurs were found to be 90 μm and 100 μm respectively. The alternate orientation of the spurs (about ±10°) is interesting and was noted first on the *Libellula* specimen.

The corresponding spurs on the underside of the hind wing of a damselfly (a *Coenagrion* from California) are shown at magnifications of 145 × and 695 × in Figs 15(a) and (b). This is the side of the wing which is exposed when the wings are folded. The spur is 60 μm high in this case and has a distinctly different shape. We have not found spurs on the upper side of the wings of damselflies, although we have not studied Lestidae which do not fully fold their wings when resting.

The heights of the spurs, which appear to be independent of chordwise position, are nevertheless more or less proportional to the wing chord. Comparative visual estimates have been made using a magnifying glass on other species (Table II).

It is possible that the spurs are bumpers to protect the wing and are smaller for smaller species to save weight. However, they are also found inside the pleats which makes the hypothesis less plausible.

TABLE II. Spur height for various species

Species		Height of spur above membrane (k μm)	Local chord at nodus (c mm)	Semi-span of wing (mm)
Aeschna Interrupta and *Eremita*	Fore	90	10·7	47·8
	Hind	100	13·7	45·7
Libellula Quadrimaculata	Fore	≃80	7·9	35·6
	Hind		9·1	34·3
Gomphus	Fore	≃80	6·6	31·5
	Hind		8·6	29·7
Sympetrum	Fore	≃70	5·8	24·1
	Hind		7·4	22·9
Anax Junius	Fore	≃125	10·2	49·5
	Hind		13·7	48·3
Coenagrion	Hind	60	4·1	25·4

(*a*)

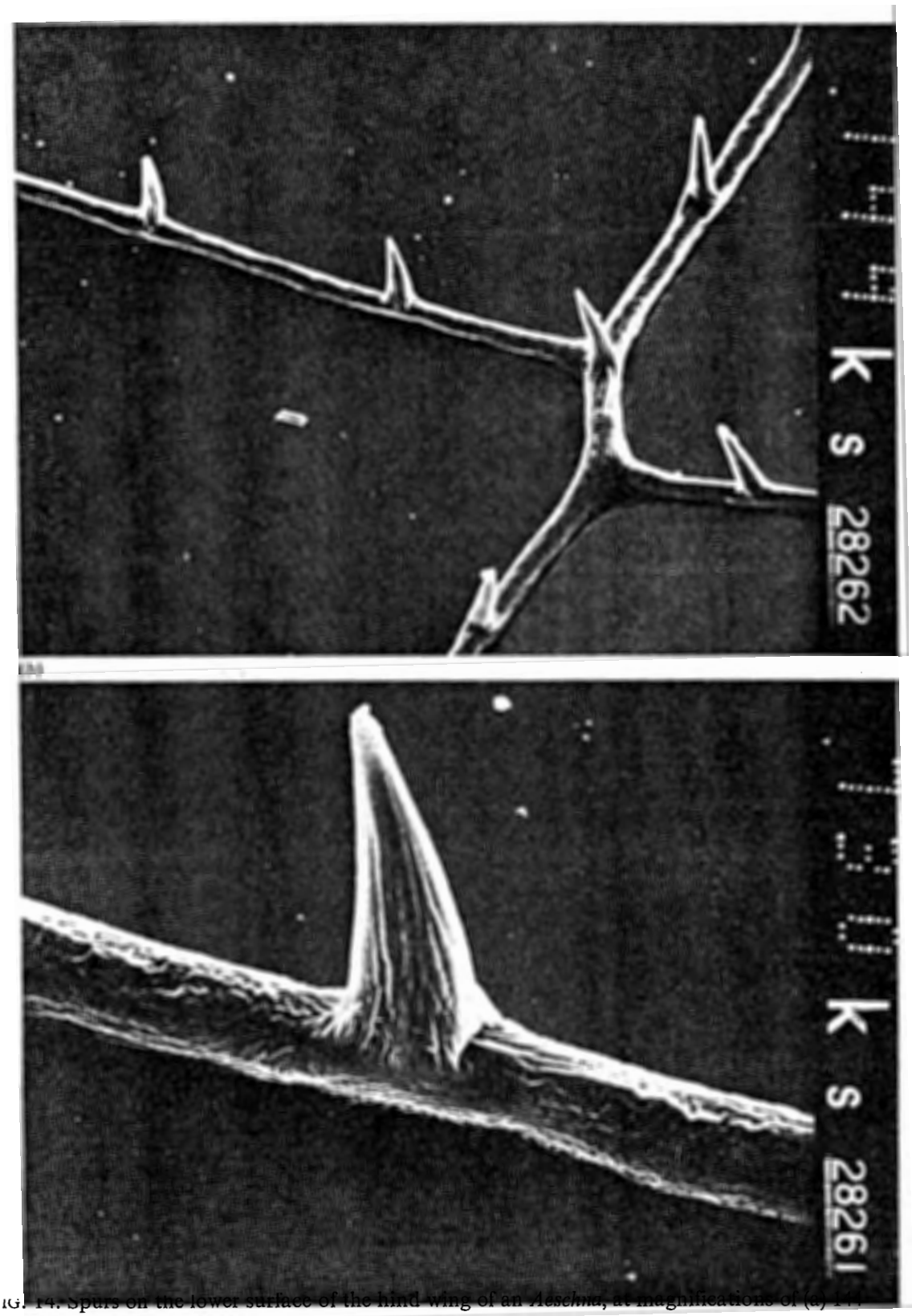

FIG. 14. Spurs on the lower surface of the hind wing of an *Aeschna*, at magnifications of (a) 145 and (b) 730.

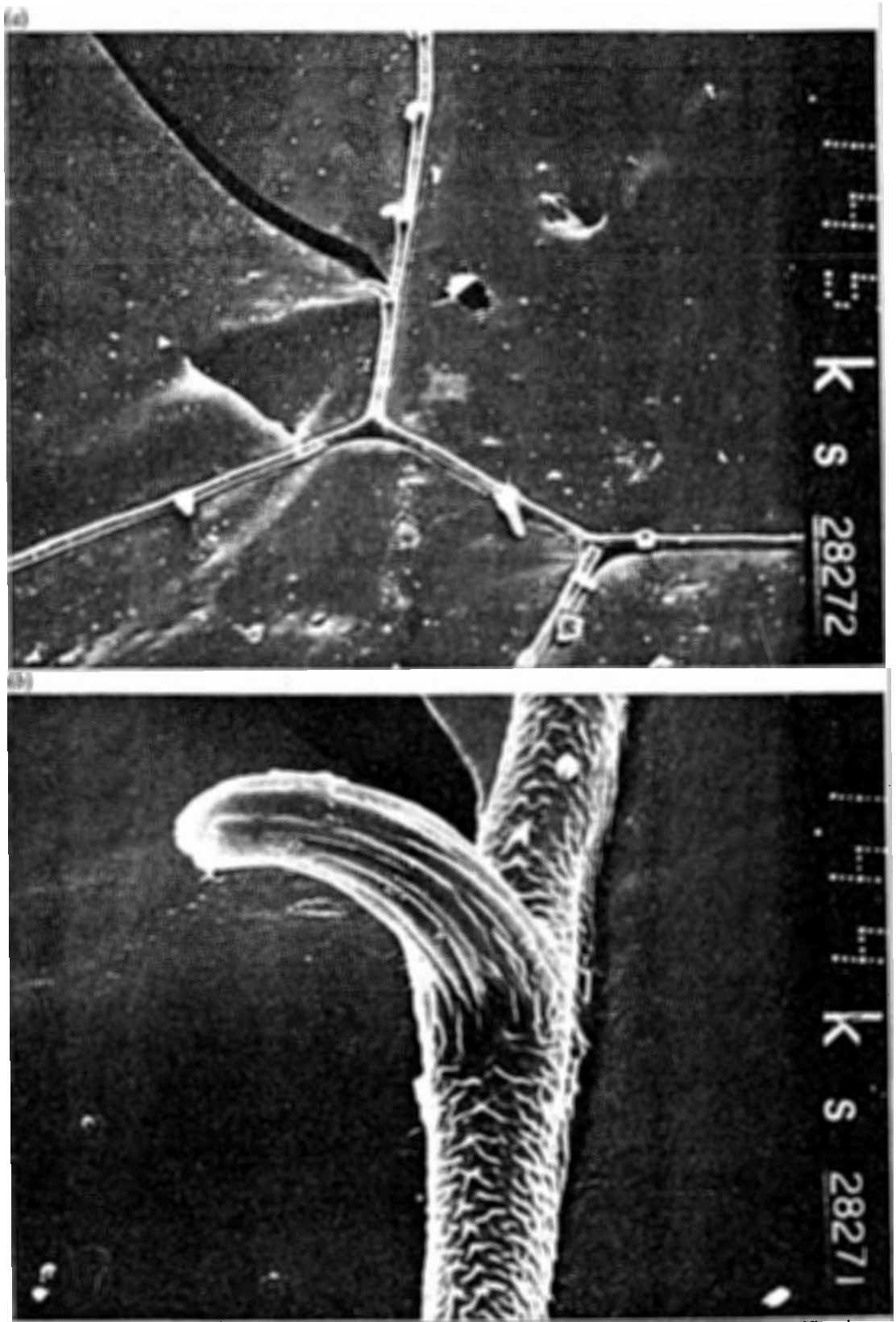

FIG. 15. Spurs on lower surface of the hind wing of a *Coenagrion*, (damselfly) at magnifications of (a) 145 and (b) 695.

Schlichting (Ref. 19, p. 617) quotes the following formula for the maximum roughness which renders a surface aerodynamically rough by protruding through the viscous sub-layer beneath the turbulent boundary layer. This is a sensitive region where the scales of Lepidoptera appear to affect the flow and reduce the drag (Nachtigall[12]). Schlichting's formula is

$$h_{\max} = 100 \frac{\nu}{U_\infty} .$$

This admissable roughness is independent of downstream distance. Taking the kinematic viscosity $\nu = 15 \times 10^{-6}\,\mathrm{m^2\,s^{-1}}$ and the typical free stream velocity of $15\,\mathrm{m\,s^{-1}}$, $h_{\max} = 100\,\mu\mathrm{m}$. It is no doubt significant that the height of the spurs for most of the cases listed is usually less than $h_{\max}$.

Pictures of the serrated leading edge along the lower arm of the costa on the hind wing of *Aeschna Interrupta* are shown at three different magnifications in Figs 16(a), (b) and (c) (60×, 246×, 1220×). In the corner of each serration there is a hairlet about 3 μm in diameter and 35 μm long which protrudes forwards and slightly ahead of the serration. Smart has identified it as a sensory macrotrichea and Weis-Fogh thought that it was there mainly for the purpose of detecting impinging objects. However, this does not

(*a*)

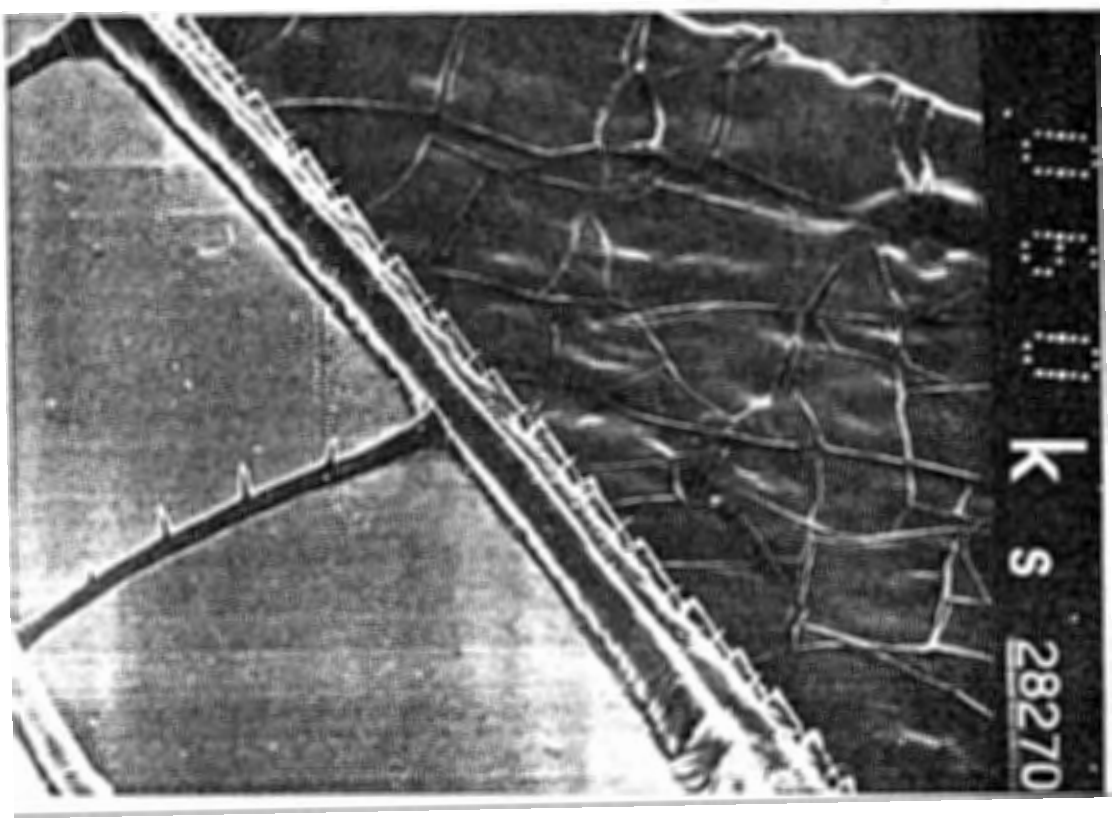

(*b*)

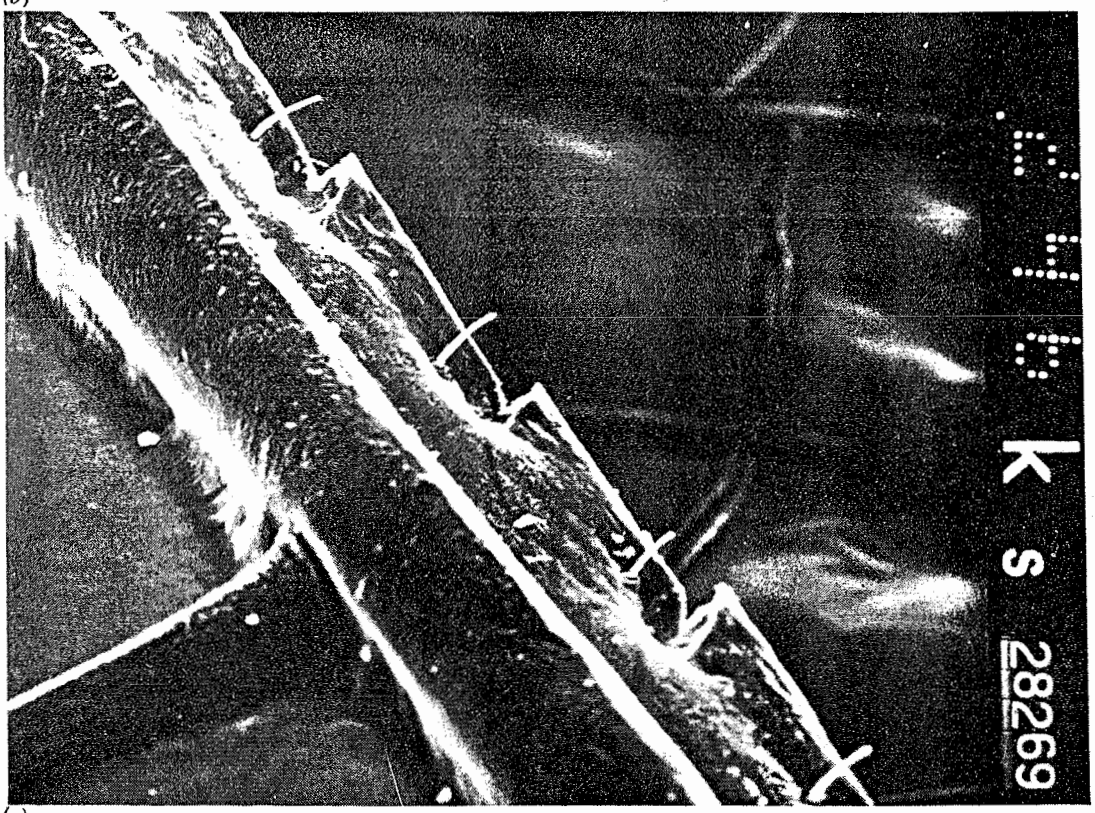

(*c*)

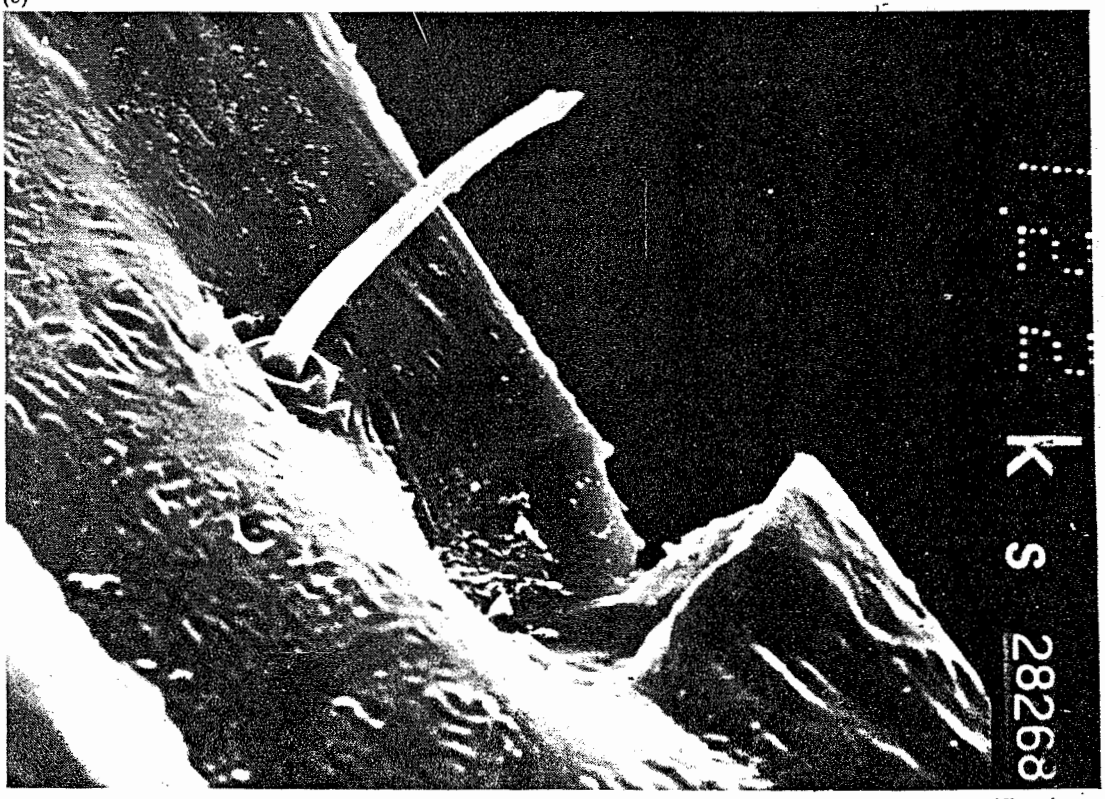

FIG 16. Leading edge serrations and hairlets on the hind wing of an *Aeschna* at magnifications of (a) 60, (b) 246 and (c) 1220.

preclude the possibility that the hairlets may also be available for sensing the airflow and that the serrations may act as turbulators to promote transition in the separated shear layer.

It might be noted that whereas the leading-edge serrations are sharp, very regular and "well-formed," the trailing edge serrations are much more irregular and rounded. This suggests that the leading-edge serrations serve to enhance transition to turbulence while the trailing-edge serrations are indentations which serve to protect the hairlets and their sockets from damage during inadvertent contact with other objects.

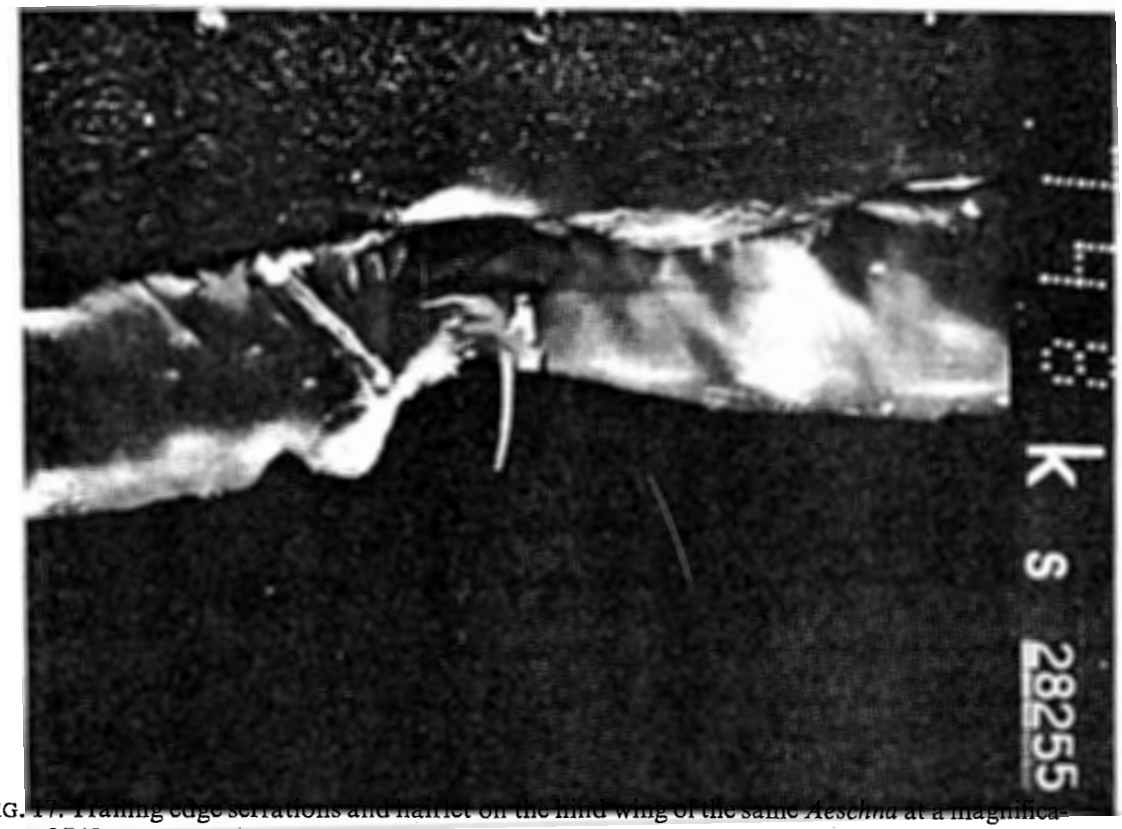

FIG. 17. Trailing edge serrations and hairlet on the hind wing of the same *Aeschna* at a magnification of 748.

It is possible that the sensory hairs at the base of the serrations in the costa have the additional role of sensing the direction of the air flow and perhaps keeping the stagnation point exactly at the leading-edge. Such a possibility would reduce the size of the leading-edge separation bubble and make it easier to understand how the bubble could be controlled on a finite wing. The entrainment underneath a large separated region may be supplied by inward flow from the wing tip and reattachment would not necessarily occur. With a small bubble confined to the pleats themselves, however, the sweeping

back of these valleys, which is a typical feature of all dragonfly wings, would provide an effective aerodynamic seal. The change of the section at the nodus also acts as a small end plate. Moreover the almost rectangular planform of the hind wing tends to reduce the wing-tip loading, especially when the wing is flapped. Thus separated regions will tend to get smaller near the tips which helps to seal the bubbles inboard. This no doubt explains the good performance of our glider which had a rectangular wing.

There may also be an aerodynamic role for the trailing-edge hairlets (Fig. 17). These are well placed to detect whether the flow leaves the trailing edge smoothly (the Kutta–Joukowski condition). They could therefore monitor the rate of incidence or camber change, which is mainly controlled by muscles attached to the leading-edge ribs, to ensure that the lift is maintained and the drag does not become unduly high. The additional information may be important in controlling the flip mechanism which Weis-Fogh[24] has described.

CONCLUSION

General

The free flight glide tests proved to be a successful method of obtaining aerofoil data free from the distorting effects of free stream turbulence. The quality of the data obtained was comparable or better than that usually obtained in full-scale flight tests but it is more scattered and requires larger corrections than data usually obtained in wind tunnels.

The unusual pleated aerofoil, in addition to being an efficient structure, has a very high aerodynamic performance. The tests with a model having a constant-chord and constant section (modelled after the dragonfly just inboard of the nodus) compared well with a very high performance, low Reynolds number, conventional aerofoil fitted with an artificial turbulator. It is probable that the actual dragonfly wing, which contains several small features not present on the test models, has an even higher performance.

Devices which *may* Improve the Aerodynamic Efficiency

The following are possibilities:

(i) The sensory macrotrichea within the serrations along the three arms of the costa may serve to detect not only foreign objects but also the airflow direction, so that the position of the leading edge stagnation point may be controlled by the root muscle and the pressure of blood within the wing.

(ii) The leading edge serrations may act to produce trailing vortices which help destabilize the separated laminar shear layer and promote transition

and reattachment. This is commonly done on model aircraft flying at somewhat larger Reynolds numbers, from about 10^4 to about 10^5.

(iii) The spurs, which appear to vary in height approximately as the first power of the wing chord from species to species, may be designed to act as anchors for the longitudinal vortices which form within the unstable shear layer downstream of separation. Such a possibility has however not yet been established experimentally and the suggestion is highly conjectural.

There is little doubt that the anatomical structure of the wing is largely determined by constraints of rapid deployment from the instar, and by structural considerations. The detailed geometry of the pleats, for example, may have no particular aerodynamic significance even though the pleats themselves may be important. They combine to make a strong main spar as the section changes in the spanwise direction. Moreover, the structure is broadly the same for all dragonflies, despite a roughly ten-fold change of Reynolds number from the largest to the smallest species, due to reduction of scale and flight speed. However, it is definitely possible that the pleats help to close the bubbles by impeding the back flow in the separated region (Wygnanski and Newman[25]), but their detailed geometric shape may be less important.

ACKNOWLEDGEMENTS

We wish to acknowledge helpful conversations with entomologists and paleontologists. Dr. John Smart of Cambridge University, Professor Vernon R. Vickery of McGill University, and the late Professor Torkel Weis-Fogh of Cambridge University. Help with scanning-electron microscopy was provided by Gunther Seibel and Dr D Sheeran, and is greatly appreciated.

REFERENCES

1. British Museum (Natural History) "Insect Flight". Leaflet No. 4, 1974.
2. Chadwick, L. E. The wing motion of the dragonfly. *Bulletin of the Brooklyn Entomological Society*, **35**, 109–112 (1940).
3. Charwat, A. F. Experiments on the variation of airfoil properties with Reynolds number. *J. Aero. Sci.*, **24**, 386–388 (1957).
4. Corbet, P. S. A Biology of Dragonflies. *In* "Aspects of Zoology". Witherly (1962).
5. Corbet, P. S., Longfield, C. and Moore, N. W. "Dragonflies". The New Naturalist Series., Collins (1960).
6. Frazer, F. C. A Reclassification of the Order Odonata. *Roy. Zool. Soc. of N.S.W.* (1957).
7. Hertel, H. Membranous Wings of Insects. *In* "Structure-Form-Movement". pp. 78–87. Reinhold (1966).

8. Hocking, B. The intrinsic range and speed of flight of insects. *Trans. Roy. Ent. Soc. London*, **104**, 225–345, (1955).
9. Imms, A. D. "General Textbook of Entomology". Methuen (1957) (revised by Richards and Davies).
10. Longfield, C. "Dragonflies of the British Isles". Worne and Co. (1949).
11. Miller, P. L. Regulation of Breathing in Insects. *In* "Advances in Insect Physiology". Vol. 3, pp. 279–344. Academic Press, London and New York (1966).
12. Nachtigall, W. "Insects in Flight". Allen and Unwin (1974).
13. Needham, J. G. and Westfall, M. J. "Dragonflies of North America (Anisoptera)". University of California Press (1955).
14. Neville, A. C. Aspects of flight mechanics in anisopterous dragonflies. *J. Exp. Biol.* **37**, 631–656 (1961).
15. Norberg, R. A. The pterostigma of insect wings, an inertial regulator of wing pitch. *J. Comp. Physiol.* (German), **81**, 9–22 (1972).
16. Oldroyd, H. "Insects and Their World". British Museum (Natural History), 3rd Ed. (1973).
17. Pringle, J. W. S. "Insect Flight". Cambridge University Press (1957).
18. Rabel, Von H. "Modellflug Profile". München (1965).
19. Schlichting, H. "Boundary-Layer Theory". 6th Ed. McGraw-Hill, New York (1968).
20. Teale, E. W. "Grassroot jungles". Dodd Mead, p. 34 (1958).
21. Tillyard, R. J. "Biology of dragonflies". Cambridge University Press (1917).
22. Weis-Fogh, T. and Jensen, M. Biology and physics of locust flight (in four parts). *Phil. Trans. Roy. Soc.* B **239**, 415–584 (1956).
23. Weis-Fogh, T. Diffusion in insect wing muscle, the most active tissue known. *J. Exp. Biol.* **41**, 229–256 (1964).
24. Weis-Fogh, T. Unusual mechanisms for the generation of lift in flying animals. *Scientific American*, **233**, 80–87 (1975).
25. Wygnanski, I. and Newman, B. G. The reattachment of an inclined two-dimensional jet to a flat surface in streaming flow. *C.A.S.I. Trans.* **1**, 3–8 (1968).